ÉCOLE DE TECHNOLOGIE SUPÉRIEURE

UNIVERSITÉ DU QUÉBEC

THESIS PRESENTED TO

L'ÉCOLE DE TECHNOLOGIE SUPÉRIEURE

A PARTIAL REQUIREMENT

TO OBTAIN A

MASTER'S DEGREE IN MECHANICAL ENGINEERING

M.Eng.

BY

MARIO GUERRA

TURBOMACHINERY TURBINE BLADE

VIBRATORY STRESS PREDICTION

MONTREAL, JANUARY 9rd, 2006

THIS THESIS HAS BEEN EVALUATED

BY A JURY COMPOSED OF :

Dr. Marc Thomas Ph.D., thesis supervisor
Mechanical Engineering Department at the École de technologie supérieure

Dr. Éric Davic Ph.D., thesis cosupervisor
Mechanical Engineering Department at the École de technologie supérieure

Dr. Azzeddine Soulaïmani Ph.D., jury president
Mechanical Engineering Department at the École de technologie supérieure

Dr. Henri Champliaud Ph.D., jury member
Mechanical Engineering Department at the École de technologie supérieure

IT WAS DEFENDED IN FRONT OF THE JURY

ON NOVEMBER 8, 2005

AT THE ÉCOLE DE TECHNOLOGIE SUPÉRIEURE

TURBOMACHINERY TURBINE BLADE VIBRATORY STRESS PREDICTION

Mario Guerra

ABSTRACT

The objective of this thesis was to develop a methodology to predict the vibratory stresses of a turbomachinery turbine blade. The aerodynamic excitation phenomenon was not studied in this research. Furthermore, the turbine blades studied in this research had the characteristics of being unshrouded, uncooled and used mainly in small to medium sized turbomachineries.

This thesis consists of four main subjects. The first subject, composed of an analysis of experimental results, was done to extract damping values of the turbine blades as well as resonances. The damping values extracted from the experimental data were used to determine analytical vibratory stresses with FLARES. Furthermore, the resonances were identified during the data reduction and therefore, the experimental vibratory stresses were extracted. These values were later used to correlate the analytical vibratory stresses predicted using FLARES.

The second subject elaborated on an analytical method with finite element analysis using contact elements to determine natural frequencies and mode shapes of the turbine blades. The new analysis with contact elements surpassed all expectations with respect to the current analysis being performed at Pratt & Whitney Canada. The natural frequencies were compared with experimental data, and were found to be in good agreement. Furthermore, the mode shapes were compared with the current analysis results, and were found to be identical.

The third subject describes an experimental method to test the blades in a controlled environment to extract natural frequencies, damping and mode shapes. The experimental testing was not performed with great success. The main deficiency was the excitable frequency range created by the high-frequency speaker.

Finally, the fourth subject compares the vibratory stress experimental values and the prediction of vibratory stresses through an analytical tool. Using the FLARES tool, the modal amplification factor was found for every resonance of the PWC Engine 1 HPT Blade, PWC Engine 2 HPT Blade and the PWC Engine 3 CT Blade. Therefore, it can be concluded that the FLARES analytical tool can predict accurate vibratory stress levels due to a resonance for an unshrouded, uncooled turbomachinery turbine blade fairly well. More work needs to be done on the CFD part of the solution to predict more accurate unsteady pressure levels at the higher engine rotating speeds.

SIMULATION NUMÉRIQUE DES CONTRAINTES VIBRATOIRES D'UNE AUBE DE TURBINE

Mario Guerra

SOMMAIRE

Dans le monde de l'aéronautique, le but principal de la recherche et développement est de réduire le poids et augmenter l'efficacité des composantes. Dans les turbomachines, une des composantes principales qui est le sujet de ces recherches est l'aube de turbine. De plus en plus, l'aube de la turbine est sollicitée en réduisant le nombre d'étage de turbine pour le même travail effectué tout en réduisant son poids. Ces aubes de turbine ont plusieurs caractéristiques vibratoires, qui à ce jour, font l'objet de plusieurs recherches avancées. Les vibrations d'une aube de turbine sont un phénomène dû à la rotation de la turbine et aux excitations aérodynamiques. Ces vibrations peuvent tomber en résonance et causer la rupture en haute fatigue d'une ou plusieurs aubes de turbine et peuvent entraîner le bris de la turbomachine pendant un vol.

Depuis plusieurs années, des méthodes empiriques et semi empiriques ont été utilisées pour faire la conception d'aubes de turbine. Ces méthodes se sont avérées inefficaces puisque plusieurs résonances ne sont identifiées qu'une fois la turbomachine testée. Certains outils numériques ont été développés pour déterminer, pendant la conception de l'aube, les résonances et les contraintes. Avec ces outils, il est ainsi possible de s'assurer que les résonances sont à l'extérieur du régime de fonctionnement du moteur. Par contre, cette méthode de conception s'avère trop conservatrice puisqu'il faut souvent changer le profil de l'aube ou augmenter sa masse pour être ainsi capable de modifier les résonances afin qu'elles ne se retrouvent pas dans un régime moteur indésirable. Donc, une méthode analytique doit être développée pour quantifier les valeurs de contraintes aux résonances, pour déterminer si l'aube de turbine doit être modifiée et pour exclure ces résonances du régime de fonctionnement du moteur. Le sujet de cette thèse est de développer une méthodologie pour prédire les contraintes vibratoires d'une aube de turbine. Il est à noter que ce mémoire portera seulement sur les effets vibratoires de l'aube. La provenance des excitations aérodynamiques ne sera pas traitée dans cette recherche.

Ce mémoire comportera quatre parties principales. Premièrement, une analyse des résultats expérimentaux de tests moteurs pour en retirer l'amortissement total des aubes ainsi que les contraintes vibratoires associées à chacune des résonances sera présentée. Deuxièmement, une méthode d'analyse par éléments finis avec des éléments de contact pour déterminer les fréquences naturelles et les modes sera présentée. Troisièmement, une analyse modale expérimentale en situation contrôlée sera effectuée sur une aube

pour en déterminer la déformée modale ainsi que la valeur de l'amortissement pour chacun des modes. Ces résultats seront comparés avec les résultats obtenus lors des tests moteurs ainsi que les résultats obtenus par les modèles analytiques. Finalement, la méthode de prédiction des contraintes de la réponse forcée de l'aube ainsi que la comparaison entre les résultats analytiques et expérimentaux seront présentées.

Dans une turbomachine, des excitations périodiques peuvent être générées à partir de plusieurs composantes internes dû à la nature rotative du moteur. Donc, lorsqu'une aube de turbine est dans la phase de conception, une attention particulière doit être portée sur ces excitations périodiques, surtout pour le stator placé en amont de la turbine, afin qu'ainsi aucune résonance n'ait lieu dans la zone d'opération normale de la turbomachine. Lors de la réduction des données expérimentales, une résonance peut être identifiée par sa très haute amplitude de contrainte comparée aux restes des fréquences et des vitesses de rotation (Figure 4). Plusieurs résonances peuvent être identifiées pour chaque mode à une fréquence naturelle spécifique, puisqu'il y a plusieurs sources d'excitations ainsi que leurs harmoniques.

Pour déterminer l'amortissement total de l'aube de turbine c-à-d., l'amortissement mécanique (matériel, frottement, etc.) et l'amortissement aérodynamique, les résultats expérimentaux seront utilisés. Cette méthode consiste à isoler la résonance identifiée pour ensuite faire épouser une courbe théorique sur celle obtenue expérimentalement. De cette façon, il sera possible d'en retirer l'amortissement total.

Les contraintes vibratoires aux résonances ainsi que l'amortissement total associé ont été obtenus pour les aubes de type Turbine de Compresseur (TC) ou Turbine à Haute Pression (THP) pour les moteurs suivant : PWC Moteur 1, PWC Moteur 2 et PWC Moteur 3. Ces valeurs d'amortissement seront utilisées pour déterminer analytiquement les contraintes vibratoires avec l'utilisation du logiciel FLARES [2]. De plus, les contraintes vibratoires trouvées serviront à titre de comparaison et calibration aux valeurs de contraintes vibratoires prédites par FLARES.

Le chapitre 4 portera sur l'application de conditions limites utilisant des éléments de contact pour déterminer les caractéristiques dynamiques d'une aube de turbine dans un environnement où le phénomène de friction est présent. Cette étude a été entreprise avec les éléments de contact disponibles dans le logiciel d'éléments finis ANSYS®. Les éléments de contact sont maillés sur toute l'aire de fixation de l'aube et du disque de la turbine pour simuler l'interaction entre les faces de contact. Aucune hypothèse n'est émise initialement sur la zone de contact entre l'aube et le disque. Les éléments de contact du logiciel ANSYS® utilisés nécessitent les valeurs des coefficients de friction dynamique et statique et d'autres paramètres qui auront un effet sur la vitesse de convergence du modèle. Avant d'effectuer l'analyse modale, une analyse statique non linéaire est effectuée en incluant les effets de précontraintes, c-à-d., la température du métal de l'aube ainsi que la vitesse de rotation de la turbine. Cette analyse statique, dite non linéaire à cause de l'ajout des éléments de contact, calcule la nouvelle position

d'équilibre de l'aube par rapport au disque dû aux effets de précontraintes. Avec la nouvelle position d'équilibre, une analyse modale, nécessairement linéaire, est effectuée dans le but de déterminer les fréquences naturelles ainsi que les déformées modales de l'aube de turbine analysée. Les quatre (4) premières fréquences naturelles de l'aube de turbine sont extraites et évaluées dans cette étude. Une étude de convergence est aussi effectuée pour déterminer quels sont les paramètres des éléments de contact qui ont la plus grande influence sur la valeur des fréquences naturelles. Les résultats expérimentaux sont extraits des tests moteurs pour les fréquences naturelles et de tests de scan laser pour les déformées modales. Il a été déterminé que le nouveau type d'analyse en utilisant des éléments de contact a surpassé toutes les attentes comparées avec l'analyse courante effectuée chez Pratt & Whitney Canada. Les fréquences naturelles ont été comparées avec les données expérimentales. La comparaison montre que les résultats analytiques et expérimentaux sont très similaires. De plus, les déformées modales, obtenues par l'analyse avec les éléments de contact, sont très comparables à l'analyse courante. Aussi, les contraintes déterminées dans les zones de contact entre les aubes et le disque ont diminué d'intensité comparée à l'analyse courante, dont une meilleure prédiction des contraintes vibratoires est à prévoir dans ces zones. Il a aussi été observé que l'aire des zones de contact augmente lors de l'analyse statique avec les effets de précontraintes, ce qui aura une signification importante pour les conditions limites du modèle pendant l'analyse modale. Finalement, une étude de convergence a été effectuée sur cinq paramètres modifiables des éléments de contact. Il a été trouvé que le modèle est stable et convergent. Par contre, la valeur du coefficient de friction a un effet significatif sur la valeur des fréquences naturelles. Des tests de pénétration entre l'aube et le disque de turbine devraient être effectués pour obtenir des valeurs expérimentales et les comparer avec les valeurs obtenues analytiquement. De plus, une étude devrait être effectuée pour déterminer si le coefficient de friction est identique ou différent pour chacun des modes de la même aube de turbine.

Pour effectuer les tests expérimentaux, une aube et un disque de turbine d'un moteur seront utilisés. Pour faire une bonne corrélation entre les résultats expérimentaux et analytiques, les conditions limites devront être très similaires. Pour les tests expérimentaux, l'aube de turbine sera assemblée dans le disque. Le disque sera soutenu par un montage spécialement conçu pour éviter ses propres fréquences de résonances dans la zone d'intérêt. Pour simuler l'effet de la force centrifuge, deux vis seront serrées dans le chanfrein du trou pour le rivet, ce qui créera une force verticale (Figure 11). Pour recréer les mêmes conditions limites sur le modèle analytique, la force centrifuge a été remplacée par un déplacement de 0,1 pouce (valeur approximative) dans le chanfrein du trou pour le rivet, dans les directions axiale et radiale (Figure 12). Lorsqu'on effectue une analyse modale expérimentale, normalement un marteau est utilisé pour exciter la composante et un accéléromètre est utilisé pour enregistrer le signal de réponse de la composante. Ceci n'est pas un problème lorsque la composante a une masse beaucoup plus significative que l'accéléromètre. Dans notre cas, l'aube de turbine a une masse inférieure à dix (10) fois la masse de l'accéléromètre. Donc, pour éviter un changement dans les fréquences naturelles dû à la masse de l'accéléromètre, un vibromètre au laser

PolyTec sera utilisé (Figure 13). Le vibromètre au laser enregistrera neuf (9) points différents sur l'aube de turbine. De cette façon, la déformée modale sera créée avec une plus grande précision (Figure 14). Pour exciter l'aube de turbine, au lieu d'un marteau typique, un haut-parleur à haute fréquence, modèle JBL Série Professionnel No. 2425, couplé à un cône, modèle No. 2306, sera utilisé (Figure 15). Un générateur de fréquence sera utilisé pour créer un signal sinusoïdal avec une plage de 2000 à 20 000 Hz. Le générateur de fréquence est branché à un mixeur Mackie Série Micro 1202-VLZ et ensuite à un amplificateur TOA Corporation Dual Power Amplifier Model: IP-300D duquel la sortie est branchée au haut-parleur à haute fréquence JBL. Le système d'acquisition de données utilisé est un Zonic Médaillon, avec 8 canaux de 0 à 20 kHz. La sortie en vitesse du vibromètre au laser est directement branchée à un des canaux du système d'acquisition de données. La sortie du haut-parleur est captée par un microphone avec une extrême sensibilité qui est placé très près de l'aube de turbine. Le microphone est branché à un des canaux du système d'acquisition de données. Les paramètres du système d'acquisition de données sont modifiés pendant les tests expérimentaux pour obtenir la meilleure résolution en fréquence pour la plage de 2000 à 20 000 Hz. Le logiciel d'acquisition de données génère une fonction de réponse en fréquence (F.R.F.) en divisant le signal provenant du vibromètre par le signal provenant du microphone. Les parties réelle et imaginaire de la F.R.F. seront utilisées pour déterminer les fréquences naturelles et la déformée modale associée.

Les tests expérimentaux n'ont pas été concluants. Le problème principal était que la plage de fréquence excitée n'était pas assez large pour avoir un signal pour tous les modes. Le haut-parleur, JBL Série Professionnel Modèle No. 2425, couplé à un cône, Modèle No. 2306, avait la capacité d'exciter une plage de fréquence allant de 3500 à 8000 Hz. Les prédictions analytiques démontraient que les quatre premiers modes de l'aube de turbine testée étaient dans la plage de fréquence allant de 3000 à 17 000 Hz. Donc, les résultats pour les modes 2, 3 et 4 sont questionnables. De plus, la cohérence du signal montrait des lacunes à de multiples fréquences dues au manque d'excitation provenant du haut-parleur. Par contre, 9 modes ont été extraits des données expérimentales. Les quatre modes analytiques ont très bien corrélé avec les résultats expérimentaux en terme de fréquence naturelle et de déformée modale. Par contre, puisque les données expérimentales sont questionnables, dues à la petite plage de fréquences excitées, l'extraction de l'amortissement modal n'a pas été effectuée.

Les aubes de turbine sont sujettes à des contraintes vibratoires dues à des écoulements turbulents dans la trajectoire des gaz de la turbomachine. La turbulence dans l'écoulement induit différentes forces sur l'aube de turbine. Lorsque la fréquence de l'instabilité est égale avec une des fréquences naturelles de l'aube, une résonance est créée avec laquelle de hautes contraintes vibratoires sont associées. Cette problématique est aussi appelée l'aéroélasticité. Plusieurs sources d'écoulement instationnaire existent dans une turbomachine, comme :
> Sillage d'aube de turbine / de stator
> Champ potentiel d'aube de turbine / de stator

➢ Vortex en bout d'aube de turbine

La plupart des écoulements instables sont circonférentiellement périodiques et sont des multiples de la vitesse de rotation de la turbomachine.

Pour prédire analytiquement les contraintes vibratoires d'une aube de turbine, la solution de l'analyse modale ainsi que la solution de la dynamique du fluide (FD) à la vitesse de rotation où la résonance est située, doivent être couplées. La solution FD n'est pas présentée dans cette étude, mais en résumé, une solution FD Euler est exécutée pour déterminer l'écoulement permanent et ainsi calculer l'amortissement aérodynamique. La partie instable de l'écoulement est déterminée avec les équations de Navier Stokes où un modèle turbulent est introduit dans le modèle. Les solutions de l'écoulement stable et instable (vs. temps) sont requises pour déterminer la force aérodynamique sur l'aube de la turbine.

En utilisant le logiciel FLARES, le facteur d'amplification modal a été obtenu pour chacune des résonances des aubes de turbine des moteurs PWC Moteur 1, PWC Moteur 2 et PWC Moteur 3. Pour déterminer les contraintes vibratoires, la matrice des contraintes vibratoires obtenues lors de l'analyse modale pour une résonance particulière est multipliée par le facteur d'amplification modal obtenu avec FLARES. La matrice de contrainte vibratoire est déterminée avec ANSYS en utilisant la valeur maximum des contraintes S1 ou S3 à chacun des nœuds et ensuite en affichant les valeurs à l'échelle. Pour s'assurer de la validité des résultats, la déformée modale extraite par FLARES a été comparée à la déformée modale obtenue avec ANSYS. De plus, l'ampleur de la force modale a été révisée pour chacune des harmoniques de l'excitation. Après investigation, il a été déterminé que le code FD ne pouvait pas prédire l'écoulement instationnaire à très haute vitesse due à des effets non linéaires basés sur le nombre de Reynolds. Donc, le niveau des contraintes vibratoires, dues à la résonance entre le deuxième mode et la première harmonique de l'excitation provenant du stator en amont, a été prédit avec une marge d'erreur allant de 0% à 371%. Le niveau des contraintes vibratoires, due à la résonance entre le quatrième mode et la deuxième harmonique de l'excitation provenant du stator en amont, a été prédit avec une marge d'erreur allant de 0% à 94%. Donc, en résumé, l'outil analytique FLARES peut prédire des contraintes vibratoires avec une bonne précision pour des aubes de turbine sans refroidissement. Par contre, plus d'études sont nécessaires sur la solution aérodynamique pour prédire des niveaux de pression instationnaire plus correctement à des vitesses de rotation très élevée de la turbomachine.

En conclusion, cette thèse comportait quatre aspects importants. Le premier objectif a été d'extraire des données expérimentales, les résonances, les contraintes vibratoires et les amortissements totaux. Cet objectif a été atteint grâce à l'élaboration d'un programme MATLAB pour extraire l'amortissement total. Le deuxième objectif a été d'élaborer un nouveau modèle par élément finis pour déterminer les fréquences naturelles ainsi que les déformées modales analytiquement. Avec l'utilisation des

éléments de contact pour simuler l'interaction entre l'aube de turbine et le disque, cet objectif a aussi été atteint. Le troisième objectif a été de déterminer les fréquences naturelles, les déformées modales et l'amortissement mécanique d'une aube à l'aide d'un banc d'essai expérimental. Cet objectif n'a pas été atteint du à la petite plage de fréquence d'excitation. Finalement, le quatrième objectif a été de prédire les contraintes vibratoires analytiquement d'une aube de turbine. Avec l'utilisation du logiciel FLARES, cet objectif a été atteint puisque les contraintes vibratoires prédites ont été comparées avec les résultats expérimentaux avec un pourcentage d'erreur acceptable.

ACKNOWLEDGEMENT

I would like to express my gratitude towards my supervisor, Dr. Marc Thomas, and co-supervisor, Dr. Eric David, for their support and teachings. Without their help, this study would have taken far longer to be completed. Futhermore, the jury members should be noted for their time and effort to make this thesis more complete.

I would like to acknowledge my coworkers at Pratt & Whitney Canada for their help and support on this project. Hopefully, this work will help us understand more about turbine blades and therefore improve our design activities.

Also, I would like to thank the « Centre de Recherche Industriel du Quebec » (CRIQ) for their help and donation of the high-frequency speaker used during the experimental testing.

Finally, I would like to specially thank my fiancée for all of her support and help throughout this endeavor.

TABLE OF CONTENTS

Page

LIST OF TABLES

LIST OF FIGURES

LIST OF ABBREVIATIONS AND SYMBOLS

HPT	High pressure turbine
CT	Compressor turbine
HCF	High cycle fatigue
CFD	Computational fluid dynamics
SDOF	Single degree of freedom
SGT	Strain gage test
CF	Centrifugal force
MU	Dynamic coefficient of friction
FKN	Contact stiffness factor
FTOLN	Penetration tolerance factor
FACT	Ratio between the static and dynamic coefficient of friction
DC	Decay coefficient
P&WC	Pratt & Whitney Canada
FEM	Finite element model
F.R.F.	Frequency response function
WF	Waterfall
EO	Engine order
OA	Overall

$[C]$	Structural damping matrix
D	Equivalent static stress or strain (static deflection)
F	The modal amplification factor
$\{F\}$	Nonlinear centrifugal force vector
$\{F(\overline{u},\Omega)\}$	Nonlinear centrifugal force
$[K]$	Geometrically nonlinear stiffness matrix including centrifugal stiffness and softening
$[K(\overline{u},\Omega)]$	Geometrically nonlinear stiffness matrix

L	Modal force
$[M]$	Structural mass matrix
N_c	Resonance speed (RPM)
N_i	Rotor speed (RPM)
$\{P\}$	Nonlinear aerodynamic force vector
$[P(\Phi)]$	Aerodynamic forces from the normal modes.
$\{q\}$	Normal or modal coordinates
t	Time (sec)
$\{u\}$	Structural position vector
$\{\bar{u}\}$	Time-averaged position
$\{\tilde{u}(t)\}$	Time dependent displacement
$\{\overline{P}(\bar{u})\}$	Time average aerodynamic forces
$\{\tilde{P}_M(\tilde{u},\bar{u})\}$	Airfoil vibratory motion dependent forces
$\{\tilde{P}_G(\bar{u},t)\}$	Unsteady aerodynamic forces caused by "gust".
X_i	Response of the component (stress or strain)

INTRODUCTION

In aeronautics, the main goal in research and development is to reduce weight and increase components efficiency. In turbomachinery, one of the main components for which a lot of research is performed is the turbine blade. The turbine blade is more and more excited by reducing the number of turbine stages required to perform the same work as well as reducing its weight. The turbine blades have multiple vibratory characteristics that have aroused many advanced research projects. The turbine blade vibrations are caused by the rotation of the blade and aerodynamical excitations. These vibrations can cause failure in high cycle fatigue (HCF) of one of multiple blades by entering in resonance, which can also cause damage to the engine and could result in an in-flight shutdown. According to the NASA/GUIde Consortium Industry Survey [1], one in-flight shutdown can cause monetary damages ranging from 500 000 to 4 000 000 $. It is also noted that 14% of engine development difficulties are due to turbine blade vibrations. Furthermore, one engine in development encounters on average 2.5 serious blade vibration problems. It is therefore easy to understand the need for studies performed on turbine blade vibrations.

For many years, empirical and semi-empirical methods have been used to design turbine blades. These methods were found to be ineffective since multiple resonances were identified only after the engine was tested. Multiple numerical tools have been developed to determine, during the design phase of turbine blades, the resonances and vibratory stresses. With these tools, it is possible to determine, with little doubt, if the resonances will be outside the normal operating range of the turbomachinery. On the other hand, this method was found to be too conservative since changes must be made to the blade to tune out resonance so that they are not situated in the operating range of the engine. Therefore, an analytical methodology must be developed to quantify vibratory stresses of a turbine blade at resonance, and to determine if the blade must be modified or will be within the material HCF capabilities. The subject of this thesis will be to develop a methodology to predict the vibratory stresses of a turbomachinery turbine

blade. It is noted that this thesis will only treat the vibratory stresses of a turbine blade. The aerodynamic excitation phenomenon will not be seen in this research. Furthermore, the turbine blades studied in this research will have the characteristics of being unshrouded, uncooled and used mainly in small to medium sized turbomachineries.

This thesis consists of four principal subjects. The first subject composed of an analysis of experimental results, which will be done to extract damping values of the turbine blades as well as resonances. The second subject will elaborate on an analytical method with finite element analysis using contact elements to determine natural frequencies and modes shapes of the turbine blades. The third subject will discuss an experimental method to test the blades in a controlled environment to extract natural frequencies, damping and mode shapes. Finally, the fourth subject will compare the vibratory stress experimental values with the prediction of vibratory stresses through an analytical tool.

CHAPTER 1

LITERATURE REVIEW

Numerous scientists have studied the unsteady aerodynamic excitation phenomenon during the past years. As per Hilbert et al. [2], the unsteady aerodynamic forces are obtained by three major sources. The first source of unsteadiness is due to the interaction between the rotating turbine blades and the turbine stator vanes. Furthermore, the circumferential non-conformities such as flow loss for other means (cooling) and the variations in the blade tip clearances are also sources of unsteadiness. The second source of flow unsteadiness comes from the turbine blade vibration adjacent to the studied blade. The third and last major source of flow unsteadiness comes from the vortex created by the blades and vanes situated upstream and downstream of the turbine blade set. Ishiara [3] performed experimental and analytical studies on the blade vibration phenomenon by concentrating his efforts on the flow unsteadiness caused by the interaction between the stator vanes and the turbine blades. To perform his study, Ishihara assumed the following three hypotheses: the two dimensional flow is incompressible, the flow instability and the blade vibrations cause the unsteady aerodynamic forces, and the speed of the flow fluctuation is inferior to the flow average speed (Figure 1).
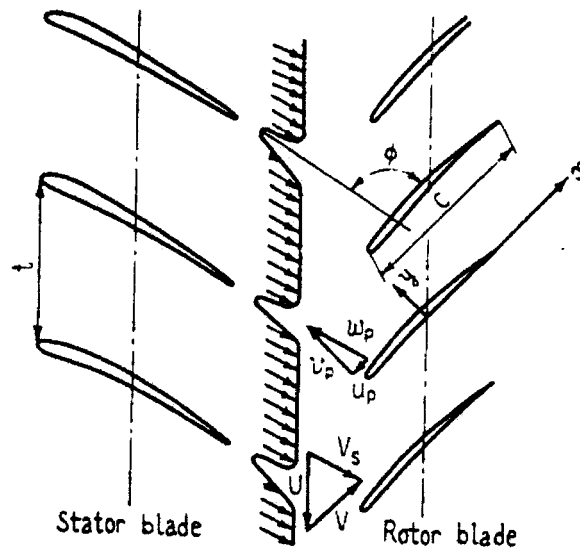
Figure 1 Aerodynamic excitation[1]

Hilditch et al. [4] performed studies on the unsteady pressures and the heat transfer of high-pressure turbines. They compared their experimental results with analytical results obtained from the program code UNSFLO. UNSFLO is a numerical simulation code to obtain results of two-dimensional unsteady pressures and it is used by multiple companies that design and build turbomachine engines. Krysinski et al. [5] also performed studies on three-dimensional unsteady flows. They experimentally investigated the effects on the performance of the turbine blades in regards to the angular positioning of the stator vanes. Jöcker et al. [6] performed studies on the influence of certain parameters of the parametrical excitations caused by the stator vanes on the high pressure turbine blades. Clark et al. [7] performed Computational Fluid Dynamics (CFD) analyses in three dimensions during the design process of a turbine blade with the goal of predicting with more accuracy the unsteady aerodynamic forces.

---

[1] Reference [3], p. 6

A chapter of this thesis will define a finite element model using contact elements to predict the natural frequencies and mode shapes of a turbine blade. Meguid et al. [8] performed analyses with finite element modelling of the turbine fixation zone. However, these analyses were performed in the static domain to obtain the stress patterns and values. They compared their results with experimental results provided by photo-elastic testing. The type of contact elements that will be used are the ones available in ANSYS® and therefore will only be the ones used in this thesis. The contact elements that will be used must be three-dimensional and must be able to consider the friction phenomenon. The friction contact elements used in ANSYS® are based on the mixed variational principles. Cescotto et al. [9] have presented an original approach to the numerical modelling of unilateral contact by the finite element method. The alternative solution that Cescotto et al. have found was to discretize independently the contact stresses and the displacement field on the solid boundary. « It is based on a mixed variational principles and allows controlling the average overlapping between the solid boundary and the foundation. In other words, a node which is not yet in contact but only close to the contact is 'informed' by its neighbours that contact is going to occur soon. »[2] (Figure 2)

Deformable solid

Gauss integration point

Contact segment

Target segment

Rigid/deformable body
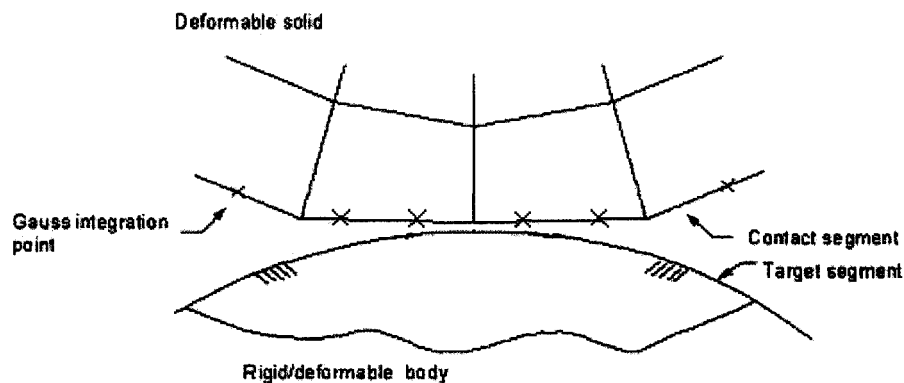
Figure 2   Solid versus foundation

---

[2] Reference [9], p. 1681

« The finite elements are based on the penalty method for solving the unilateral contact and slip conditions and on the Coulomb model for the friction strength. When slipping contact appears, the constitutive equation of the contact element is unsymmetrical. Therefore, an unsymmetrical solver is used. »[3] This method is currently being used in ANSYS® to solve model which uses contact elements. In addition, Berger et al. [10] created a user-programmed function in ANSYS® to perform analyses of microslip damping on a turbine blade. They have created a "superelement" that would replace the contact elements currently used in ANSYS®. This new element contains a friction traction law definition based on the Coulomb friction model and a stick-slip transition logic based upon the force and velocity conditions. Although is still uses the contact elements from ANSYS® to determine the initial contact phase, the computational time per load step is greatly reduced. The overall energy dissipation, stresses and interface tractions are more accurately predicted. There are two reasons for which this methodology will not be used in this thesis. First, this macro is not yet available for the public. Second, the "superelement" in a two dimensional problem, while the fixing a turbine blade is a three dimensional problem.

A chapter of this thesis will describe a modal testing procedure to determine the natural frequencies and mode shapes of a turbine blade using an acoustical excitation. Li et al. [11] performed such experiments on an advance bladed disk prototype. The reason for an acoustical excitation is to produce a non-contacting measurement system and therefore, not affecting the system response. The measurement of the excitation is done using a calibrated microphone, while the measurement of the disk response is done with a Single-Point Laser Vibrometer (SPLV) and a Scanning Laser Doppler Vibrometer (SLDV). The speaker generates a signal, which excites the disk blades at their natural frequencies. Using the microphone, the sound pressure level is recorded so that a Frequency Response Function can be obtained. Li et al. used a travelling excitation wave

---

[3] Reference [9], p. 1682

to excite all the blades of the disk. In this thesis, only one blade will be tested and therefore, a single speaker excitation will be needed.

Jay et al. [12] performed studies on turbine blades forced response. By performing experimental testing, they were able to identify the dynamic responses resulting from the interaction between the stator vanes and the turbine rotor blades. Furthermore, they performed an analytical description of the aerodynamic force originating in the difference between the number of stator vanes and the number of turbine blades. Moffatt et al. [13] also performed the same studies as Jay et al. [12], although using the program ANSYS® to determine the natural frequencies and mode shapes of the studied turbine blade and interpolated the results with the CFD meshing. The Navier-Stokes equations were resolved in the frequency domain by using a one-vane passage approach to obtain the aerodynamic excitation and the damped forces. This method was based on single-degree-of-freedom (SDOF) assumptions. Ultimately, Hilbert et Al. [2] performed the same studies on forced response in a three-dimensional field. The analysis consisted in a three-dimensional multi-stage turbine in which the stable and unstable dynamic fluid response was determined. A non-linear structural analysis and a linear dynamic analysis were performed to determine the displacement amplitude of the blade in resonance during the engine run. By combining a structural analysis and a dynamic analysis with a the fluid dynamic analysis, an iterative solution to the aeroelastic problem was obtained (Figure 3).
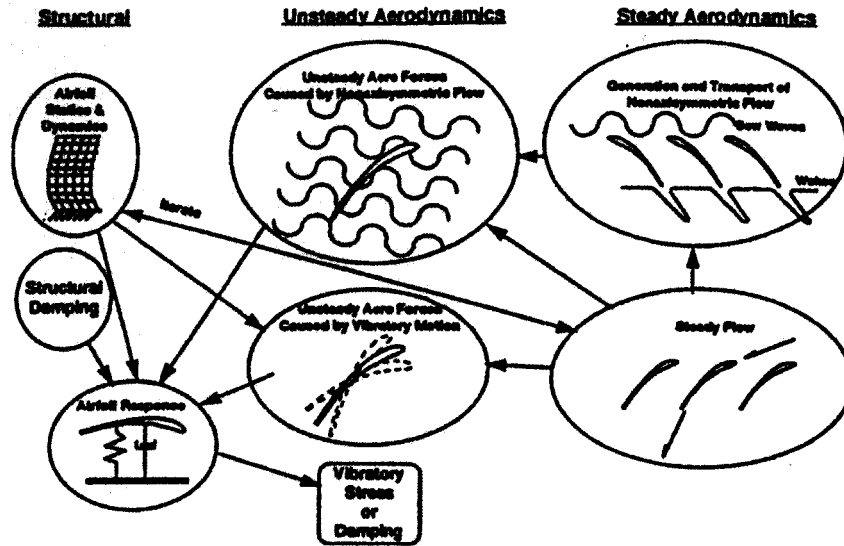
Figure 3   Method to predict the forced response of a turbine blade[4]

Busby et Al. [14] already performed studies on the axial blade spacing effect and determined that the increase in total relative pressure loss of the turbine blade was eliminated by the decrease in total relative pressure loss of the stator vane when the axial spacing was decreased. Furthermore, the predicted decrease in pressure loss of the stator vanes with the decrease in the axial spacing is mainly due to the reduction in wake mixing loss. Finally, the predicted increase in the total relative pressure loss of the turbine blade with a decrease of the axial spacing is mainly due to the increased interaction between the wakes produced by the stator vanes with the turbine blades.

---

[4] Reference [2], p. 2

CHAPTER 2

OBJECTIVES AND METHODOLOGY

The forced response prediction, with accuracy, of the turbomachinery turbine blade forced response will be studied throughout this thesis. The turbine blades studied will be uncooled and unshrouded. The thesis objectives will be the following:

- ➢ Extract the total damping based on experimental data.
- ➢ Create a finite element model using contact elements for more accurate boundary conditions.
- ➢ Experimentally measure the natural frequencies, modes shapes and mechanical damping values.
- ➢ Create a methodology to predict vibratory stresses in the turbine blade.

To extract the total damping of the turbine blade, meaning the mechanical damping (material, friction, etc.) and the aerodynamical damping, the experimental data from previous tests will be used. This method consists in isolating the identified resonance and fit a theoretical curve over the experimental data. Using this theoretical curve, the total damping will be extracted. For the finite element model, a three-dimension turbine blade model and part of the disc will be meshed. No hypothesis will be made on the localization of the contact surface between the turbine blade and the disc. Therefore, the whole fixation zone of the blade and the disc will be meshed with contact elements. The finite element model will determine the natural frequencies and the mode shapes of the turbine blade. The analytical results will be compared to the experimental results. For the experimental testing, a laser vibrometer and an acoustic excitation will be used to determine the natural frequencies, modes shapes and extract the mechanical damping values. For the prediction of the vibratory stresses method, the FLARES [2] code will be used to superimpose the aerodynamic forces onto the turbine blade. From this, the modal participation factor will be obtained. This factor will multiply the modal stress vector obtained by the finite element model so that, finally, the vibratory stresses of the turbine

blade can be obtained. Most of the work will be on the parametric study to obtain consistent stress values from FLARES and ANSYS®.

CHAPTER 3

STRAIN GAGE TEST DATA EXTRACTION

Experimental data has to be extracted from a Strain Gage Test (SGT) so that HCF (High Cycle Fatigue) lifing can be performed on the required blade. In addition, in this research project, the experimental data has to be extracted so that it can be correlated with the analytical results. Furthermore, to obtain the vibratory stresses analytically, the damping value has to be extracted from the data reduction since it cannot, currently, be calculated analytically. The data reduction will be done only on the high-pressure turbine blade for turbofans engine and the compressor turbine blade for the turboprops engines. The data reduction will be performed on the high-pressure turbine blade of the PWC Engine 1 and PWC Engine 2 engines, and on the compressor turbine blade of the PWC Engine 3 engine. These blades are uncooled, unshrouded (no inter-connection between blades) and the data extrapolated are only to be used on blades with the same characteristics for design. Furthermore, a damping value trend will be extrapolated as function of mode, natural frequency and harmonic of excitation. It is important to note that only the modes that are in resonance or close to will be of importance and studied.

3.1 Resonance Identification

A resonance is defined as a coincidence between a natural frequency of a component and a periodic excitation on a waterfall (Figure 4). A waterfall is obtained from a Fast Fourier Transform of a time signal given by a strain gage during an engine testing. The three axes represent the following: the frequency range, the engine rotational speed and the amplitude of the vibratory strain. Every horizontal line represents one capture engine speed during the test. During the test, the strain gage captures the vibratory strain at the determine location on a blade. The blade exhibits vibratory strain due to its own natural frequencies (almost parallel to the engine rotational speed axis) or due to the excitation sources. If the excitation is an integer of the rotation speed, such as upstream vane

wakes, a diagonal line will appear on the waterfall. If the excitation line and the natural frequency line meet, a resonance will occur which is usually demonstrated by high amplitude vibratory strain.
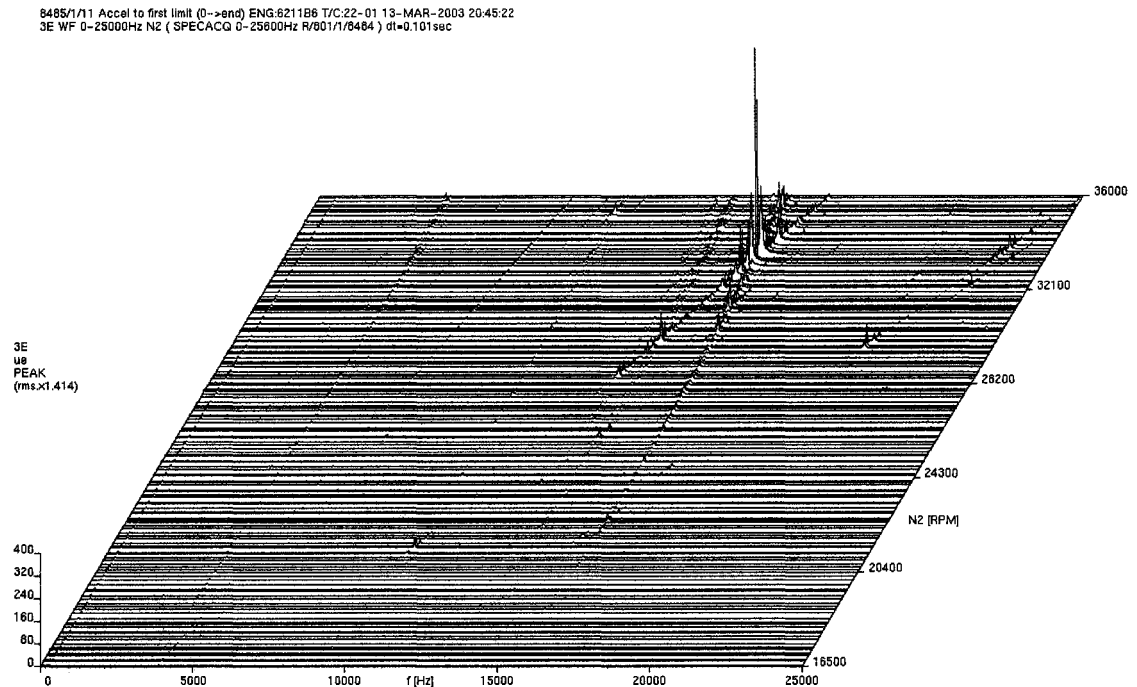
Figure 4   Waterfall 0-25000 Hz

In a turbine engine, periodic excitations can be generated by multiple components due to the rotating nature of the engine. Therefore, when designing a turbine blade, great care must be taken to the periodic excitations, mostly the vane passing, so that no resonance occur in the running range of the engine. When performing data reduction, resonance can be identified by the high amplitude of the strain compared to the rest of the frequencies and rotating speeds (Figure 4). Multiple resonances can be identified on each mode at specific natural frequency due to the different surrounding components and the excitation harmonics. The results are presented in section 7.1.1.

3.2 Modal Damping Extraction

When turbine blade vibratory stresses are predicted analytically, the total damping acting on the blade is critical to the accuracy of the stress value. The total damping is the sum of the aerodynamic damping and the mechanical damping. Furthermore, the mechanical damping comprises the structural damping of the material and the friction damping generated in the fixing area. These quantities depend on the CF load, metal temperature, frequency, material and surface finish at the blade-disc interface. The aerodynamic damping can be obtained by analytical calculations using Euler equations. As for the remaining damping values, the only accurate method to obtain them is from experimental testing. Therefore, from SGT data reduction, the total damping values have to be extracted so that the stress values can be predicted with accuracy.

The basic method to determine the total damping value is the following:

1- Identification of the resonance
2- Identification of the Engine Order range
3- Export the data
4- Curve fitting
5- Analytical tool

The identification of the resonance was presented previously (Figure 4). The goal of the Engine Order Plot is to build the blade response versus the rotor speed on an engine order excitation in order to have almost a constant force over a small rotor speed range. The Engine Order band has to be wide enough to capture the several adjacent spectral components that define the full peak. To make sure that the Engine Order Plot range is wide enough, a spectrum plot at the resonance speed is plotted from the waterfall (Figure 5).
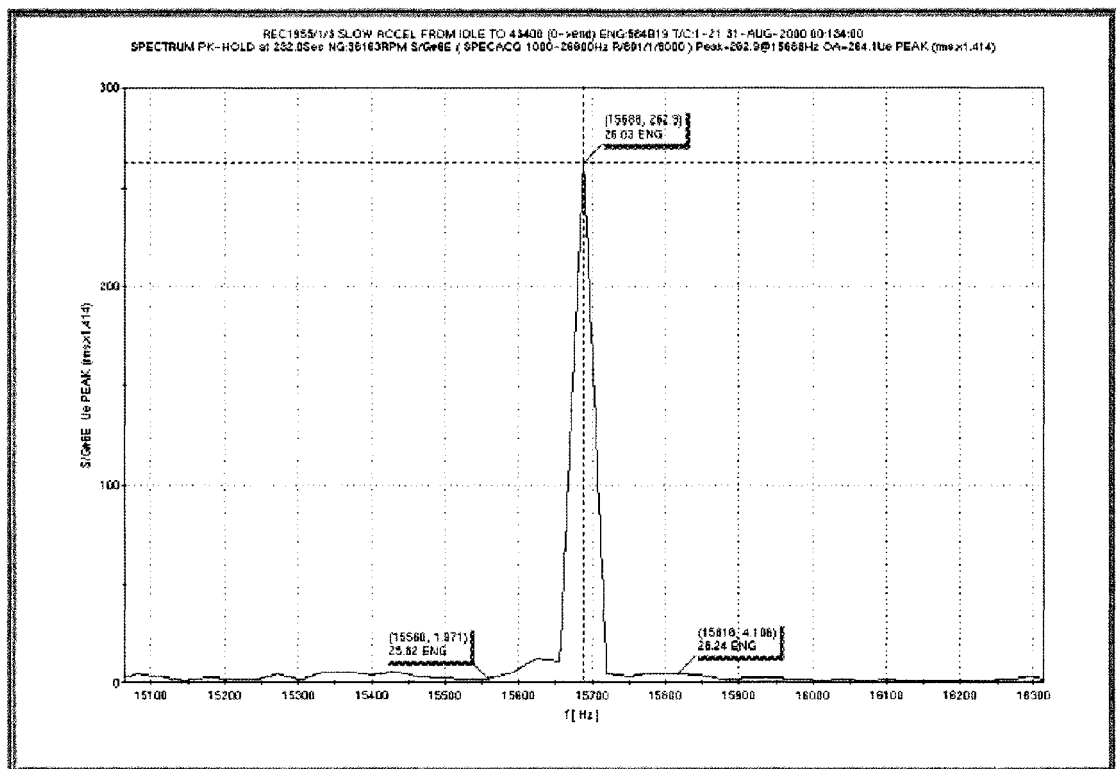
Figure 5   Resonance spectrum plot

Based on the spectrum plot, the Engine Order band is defined by incorporating the whole peak. The Engine Order Plot is relative to the engine rotor speed. To get the real resonant peak, an average over a frequency bandwidth for each engine revolution is done. To avoid any loss of information, the FFT frequency bandwidth has to be centered on the resonance frequency and has to be equal or less than 6400 Hz due to the limitation in resolution of the analyzer. Using this information, the data can be exported to an ASCII file for post-processing.

In order to extract the damping from the Engine Order curve, a single degree of freedom (SDOF) curve fitting method is used. This method is based on the viscous damping theory. As this is used locally (resonance), this is an acceptable assumption since, based

on the experimental and analytical data, if the modes are uncoupled. The response of a SDOF in the rotor speed domain is:

$$X_i = \frac{D}{\sqrt{\left(1-\left(\frac{N_i}{N_c}\right)^2\right)^2 + \left(2\zeta\frac{N_i}{N_C}\right)^2}}$$ (3.1)

D   Equivalent static stress or strain (static deflection)

ξ Damping ratio

N_c Resonance speed (RPM)

N_i Rotor speed (RPM)

X_i Response of the component (stress or strain)

As the rotor speed range is known (N_i), the function X_i will be fully defined when D, N_c and ζ are known. The aim of the curve is to find D, N_c and ζ that best define a SDOF fit for the SGT data [15]. The least square method is used to achieve this.

The least square function is defined as:

$$\Pi(\zeta, N_c, D) = \sum_i (Y_i - X_i)^2$$ (3.2)

With: X_i = theoretical SDOF curve as defined above over the rotor speed range

        Y_i = SGT data over the rotor speed range

        i = index that varies to dwell the rotor speed range of interest.

The parameters D, N_c and ζ that minimise the least square function will define the function X_i that best fit the SGT data Y_i. The damping factor ζ that is found with this method is assumed to represent the experimental damping.

A developed MATLAB® routine (APPENDIX 1) is used to fit the SDOF curve on the SGT data. This routine uses a MATLAB iterative solution. This function finds the

parameters D, N_c and ζ that minimises the least square function. It also allows the user to specify the speed range of data that have to be used in the least square function calculation. The inputs of the routine are:

Table I

MATLAB® routine inputs

MATLAB variable name	Example	Description
sgt_data	'EO_REC1955_3_6F_2H.CSV'	The .csv file that was exported from the waterfall. It contains the Engine Order data versus the rotor speed. Some percent signs have to be added at the beginning of the text lines to comment them.
Nmin	34100	Minimum speed of the range of interest.
Nmax	38900	Maximum speed of the range of interest.
Tol_damping	1E-6	Termination tolerance of the damping factor.
Tol_reso_speed	1E-6	Termination tolerance of the resonance speed.
Tol_defl	1E-6	Termination tolerance of the static deflection.
Max_iter	1E50	Maximum number of iteration.
Dratio_init	1E-3	Initial value of the damping factor.
Delta_init	1.5	Initial value of the static deflection.

The results of the MATLAB® routine present the SGT data curve superimposed with the calculated SDOF analytical curve (Figure 6).
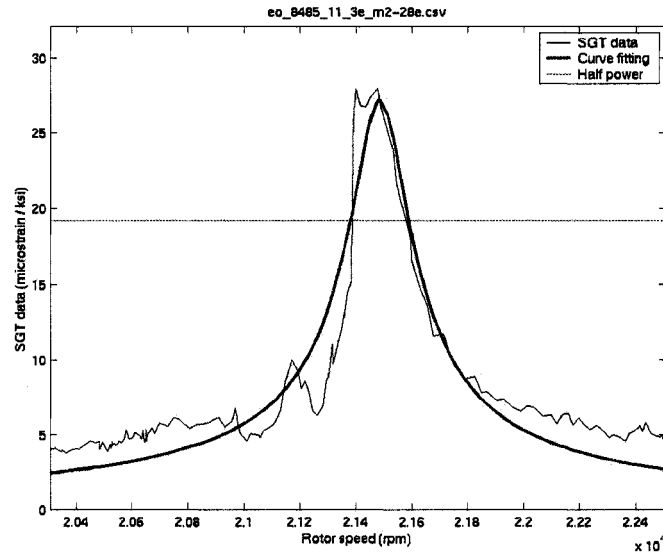
Figure 6   Curve fitting for damping extraction

The total damping value is given in the logarithmic decrement form. This method invokes that the forcing value throughout the resonance is constant (D parameter is constant). In reality, the force changes with regards to the engine rotating speed. Since the resonance band is very narrow (≈ 1000 RPM), the change in the forcing value is deemed negligible. The results are presented in section 7.1.2.

3.3   Vibratory Stress Calculation

The experimental stress values are determined using the Hooke's Law:

$$\{\sigma\} = \{E\} \, \{\varepsilon\} \tag{3.3}$$

The deformation or strain (ε) is obtained from the data reduction plots. Since it is assumed that the highest stress value will be at the surface of the turbine blade, only one strain gage (one direction) is necessary to determine the vibratory stress. The Young's modulus (E) is dependent on three parameters. The first parameter is the type of material used for the turbine blade since different materials have different Young's modulus. The second parameter is the metal temperature of the blade at the location of the strain gage

position. The Young's modulus decreases with the temperature elevation and therefore accurate temperature values are needed. The third parameter is the orientation of the strain gage. The materials used in a turbine blade are generally single crystal orthotropic materials. The orthotropic characteristic suggests that the Young's modulus of the material is not equal in all the axes of the crystal. Therefore, the orientation of the strain gage must be taken into account to determine the correct Young's modulus value. The results are presented in section 7.1.3.

CHAPTER 4

FINITE ELEMENT MODEL BOUNDARY CONDITIONS DEFINITION

This subject will be concentrated on the application of boundary conditions using contact elements to determine the dynamic properties of a turbomachinery blade in an environment where the friction phenomenon is present. This study is performed using ANSYS® contact elements [18], which are meshed on the entire fixing area to simulate the interaction between the blade and the disc [16]. No assumptions were made initially for the blade-disc contact surface. The ANSYS® contact elements used require input for the static and dynamic friction coefficients and other parameters that have an effect on the convergence of the model. Before the modal analysis, a non-linear static analysis is performed with pre-stress effects, i.e. the blade metal temperature and the turbine shaft rotational speed. This static analysis, which is non-linear due to the addition of contact elements, calculates the new equilibrium position of the blade with respect to the disc due to the pre-stress effects. With the new equilibrium position found, a linear modal analysis is performed in order to obtain the natural frequencies and mode shape of the analyzed blade. The first four (4) natural frequencies and mode shapes are evaluated in this study. A convergence study is also performed to determine which contact element parameters have a significant influence on the natural frequencies values. The experimental results are extracted from strain gage tests for the natural frequencies and from a laser scan tests for the mode shapes. The analytical results are compared to the experimental results. Furthermore, experimental testing will be performed to determine the correct friction coefficient values as well as mode shape determination.

Contact elements are primarily used to simulate the contact stress and displacement between two moving components relative to each other. Current turbomachinery blade modal analyses are performed in PWC without the mating disc. The new method will

include part of the disc, and the contact elements will be used between the blade and the disc fixing.

4.1 Current Analysis

The current analysis omits the displacement between the blade and the disc and assumes no motion of the blade. The turbine blade is meshed using tetrahedral 10-node parabolic elements (SOLID92). These analyses typically have approximately 40,000 elements, 60,000 nodes and 180,000 degrees of freedom. The boundary conditions consist of zero displacement in the radial and tangential directions at the supposed contact line and zero displacement in the radial and axial direction for the front and rear fixing planes of the blade (Figure 7).
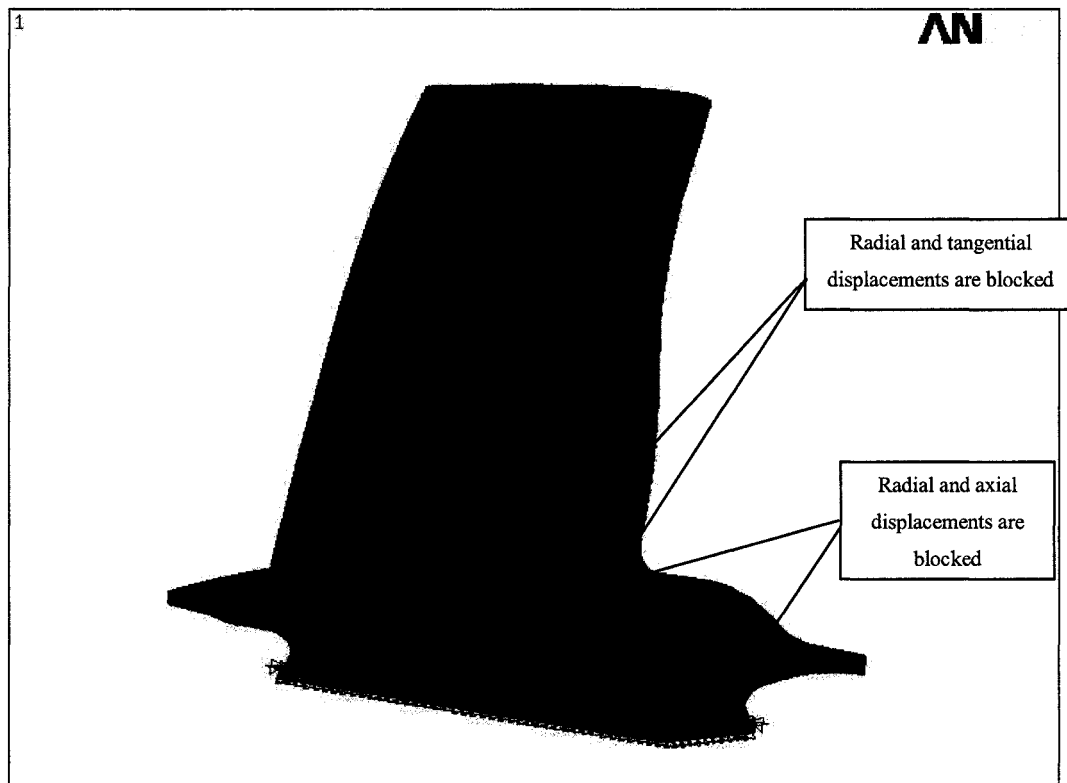
Figure 7   Blade fir-tree line blockage

A static analysis is performed including pre-stress effects such as centrifugal force (rotation) and temperature. The static analysis determines a new mass [M] and rigidity [K] matrices due to the deformation of the blade. Once the static analysis is completed, a modal analysis is performed using the updated matrices. The results from this modal analysis are natural frequencies and mode shapes. Due to the total blockage contact line, there are peak stresses present in the fir-tree area, which do not reflect the reality (Figure 8).
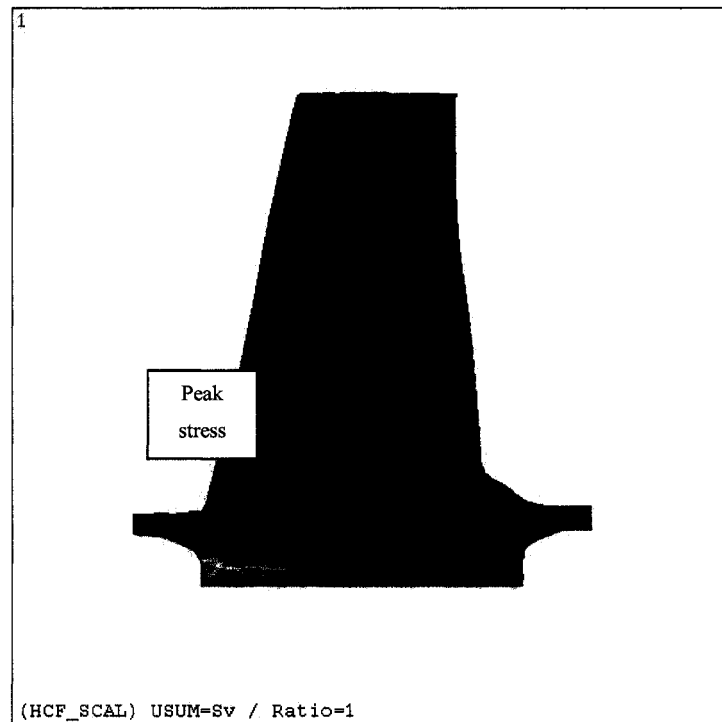
Figure 8   Blade stress with contact lines blocked

The unrealistic stress in the fir-tree area is the main reason for a more realistic modeling using contact elements. The vibratory stress can cause severe damage, which can extend up to the fracture of the blade, at the fir-tree area. Therefore, it is very important to be able to predict with more precision the stresses in that particular region.

4.2 New Analysis

The new analysis will be performed in much the same way, as is the current analysis (section 4.1). A static and modal analysis will be performed sequentially. The difference will be in the boundary conditions settings. In the new analysis, blockage of the blade will not be assumed. Contact elements will be used over the entire fir-tree area, and the static analysis will determine whether displacement occurs. To perform an ANSYS® three-dimensional static contact analysis, two types of elements must be used. The contact element (CONTA174) is used to represent the contact and sliding between the 3-D "target" surfaces and a deformable surface, defined by this element. CONTA174 is an 8-node element intended for general rigid-flexible and flexible-flexible contact analysis. The contact detection points are located either at the nodal points or at the Gauss points. The contact element is constrained against penetration into the target surface at its integration points. However, the target surface can penetrate through into the contact surface. The "target" surface is a geometric entity in space that senses and responds when one or more contact elements move into a target surface. The target element (TARGE170) is used to represent various 3-D target surfaces associated with contact elements. The "contact-target" pair concept has been widely used in finite element simulations.

4.3 Meshing of Contact Elements

The meshing of the components is performed using CATIA®. The section of the disc and the fir-tree region of the blade are meshed using 20-node hexahedral elements. Because of the complex shape of the blade's airfoil, 10-node tetrahedral elements are used for meshing (Figure 9). These analyses typically have approximately 80,000 elements, 100,000 nodes and 300,000 degrees of freedom. The boundary conditions used try to reflect the reality with more accuracy than the current analysis. The sides of the

disc portion are fixed in every direction while the blade is fixed in the axial direction using the nodes on the rivet hole to simulate the use of the rivets.
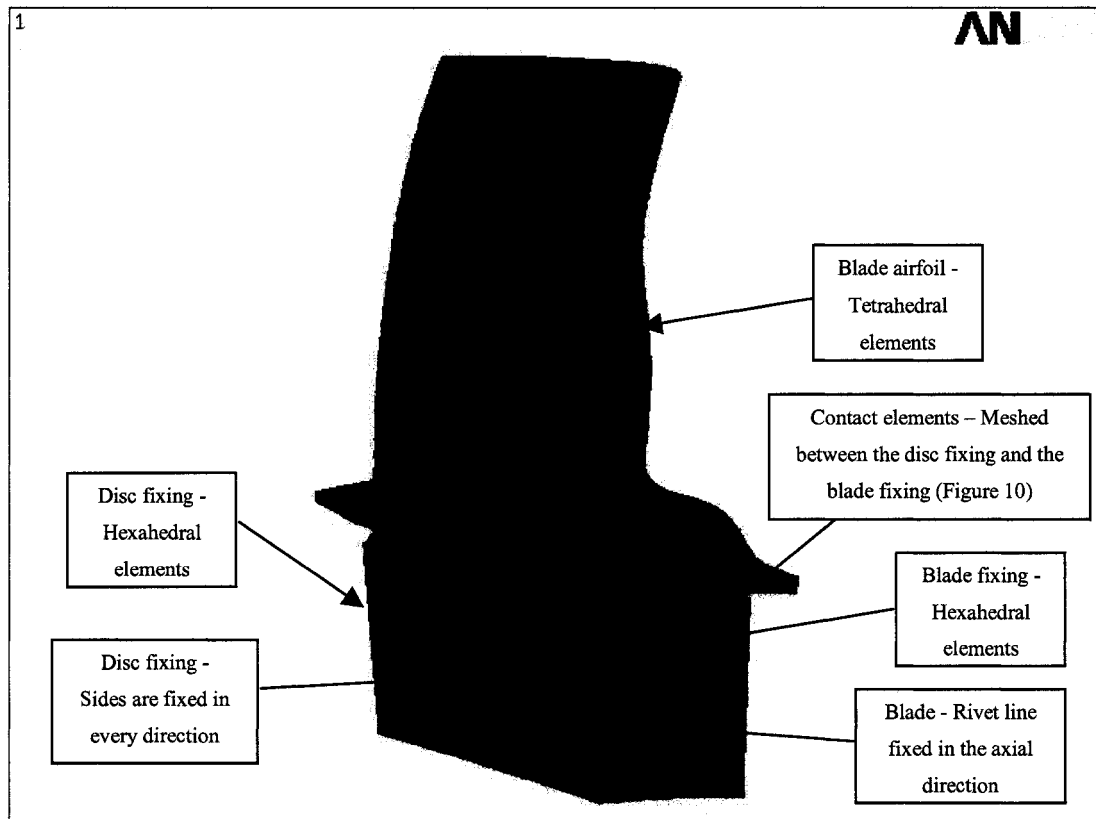
Figure 9   Blade and disc meshing

The meshing of the contact element pairs is performed using ANSYS®. Selections of nodes of the disc and blade fir-tree region in CATIA® are created for meshing purposes in ANSYS®. The target elements (TARGE170) are meshed over the fir-tree area of the disc. There are no assumptions made with respect to the contact areas; and so the whole fir-tree is thus covered with the target elements. The same process is performed for the blade fir-tree region (Figure 10).
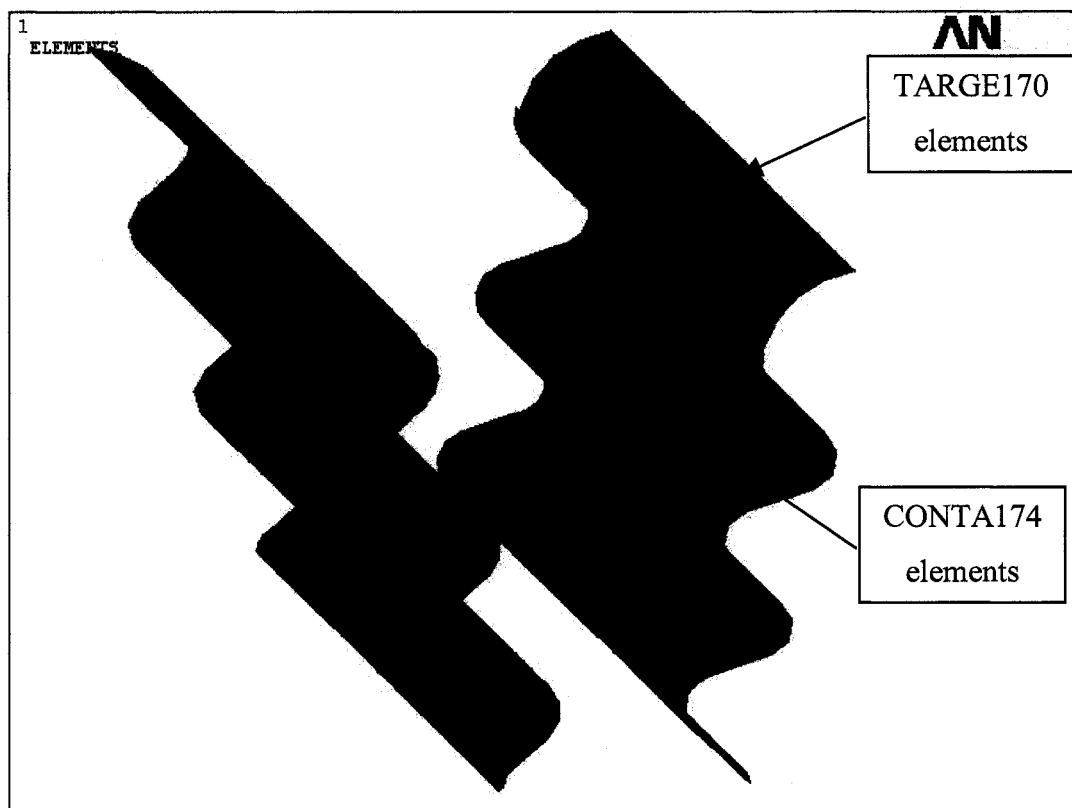
Figure 10   Contact elements mesh

Since the part of the disc has been modeled, it is jugged flexible but no penetration can occur since "target" elements are used. The different contact types of the contact elements during the static and modal analyses are presented in the table below.

Table II

Contact type for the static and modal analyses

Contact Type	Static Analysis	Modal Analysis		
		Initially Touching	Inside Pinball Region	Outside Pinball Region
Bonded	Bonded	Bonded	Bonded	Free
No Separation	No Separation	No Separation	No Separation	Free
Rough	Rough	Bonded	Free	Free
Frictionless	Frictionless	No Separation	Free	Free

Since a friction coefficient value is given to the contact elements, the "rough" contact type occurs during the static and modal analyses for this study. Therefore, after the static analysis is performed, only the elements that are touching to each other will be bonded while the contact elements pairs that are not touching will have no stiffness added.

4.4   Contact Element Input Data

The contact element pair has multiple parameters that have to be defined for the analysis to get a converged solution. The first parameter is the dynamic coefficient of friction (MU), which will have an effect on the limit shear stress and the relative sliding distance. The second and third parameters are the normal contact stiffness factor (FKN) and the penetration tolerance factor (FTOLN) respectively. These factors are related for the convergence purposes. The normal contact stiffness factor determines the penetration rigidity of the component while the tolerance factor determines whether the penetration compatibility is satisfied when using the penalty and Lagrange method. The contact compatibility is satisfied if the penetration is within a tolerance of the FTOLN value multiplied by the depth of the underlying solid. Therefore, if the FKN and the FTOLN factors are too low, the analysis will not converge due to the presence of a higher than allowed level of penetration. The fourth and fifth parameters are required for a smooth transition zone between static and dynamic friction given by the following equation [4.1]:

$$\mu = MU \times \left(1 + \left(FACT - 1\right)\exp(-DC \times V_{rel})\right) \qquad (4.1)$$

μ is the static coefficient of friction, MU is the dynamic coefficient of friction presented previously. The parameters $FACT$ for the ratio between the static and dynamic friction coefficients and DC for the decay coefficient are required. V_{rel} is the slip rate between the blade and the fixing calculated at each time step by ANSYS®. Since these parameters are not known, a convergence study has been performed and will be presented in the following chapter on these five parameters. The contact element pair

has many other parameters but they were kept at their default values since they had no effect on frequency values and mode shapes. The results are presented in section 7.2.

CHAPTER 5

EXPERIMENTAL TESTING

Experimental data is extensive at PWC. For certification purposes, all HP or CT blades have a strain gage test (SGT) performed to determine the resonances in the running range and the vibratory stress associated with them. A strain gage test is done in test cell using a real engine as a test vehicle. Strain gage are attached to any components as required by the engineer. When the engine is running, a data acquisition system records the strain gage signal as well as the engine rotating speed. A Fast Fourier Transform is performed by the data acquisition system on the strain gage recorded time signal. This step transforms the time signal into the frequency domain and using the rotating speed, a waterfall plot is generated. For a turbine blade certification, these tests require the application of strain gages on different blades, the gages being located on high strain areas based on the FEM model. Therefore, the accuracy of the mode shape is of prime importance in order to assess the HCF life of the component. Due to highly complex and expensive method of performing these strain gage tests, a static test at normal temperature is developed to further study the contact elements as boundary condition in the blade FEM model. The main goal of the experimental testing is to determine the friction coefficient for the model in order to reproduce the mode shapes at the correct natural frequency values. Furthermore, the need for a specific friction coefficient for every mode shape might arise. In addition, contact testing using chalk between the blade and disc contact faces will be applied and the results will be correlated with the FEM modelling.

5.1   Experimental Test Model

To perform the experimental testing, a blade and disc will be used. To correlate the results of the experimental testing on the FEM results, the boundary conditions have to be the same. For the experimental test, the blade will be assembled on the disc. The disc

will be held in a specially designed fixture to avoid any resonance in the frequency range of interest. To simulate centrifugal force (CF) loading, two screws are forced inside the chamfer of the rivet hole, which will create an upward force due to its conical shape (Figure 11). Refer to Figure 12 for illustration of the conical shape of the rivet hole.
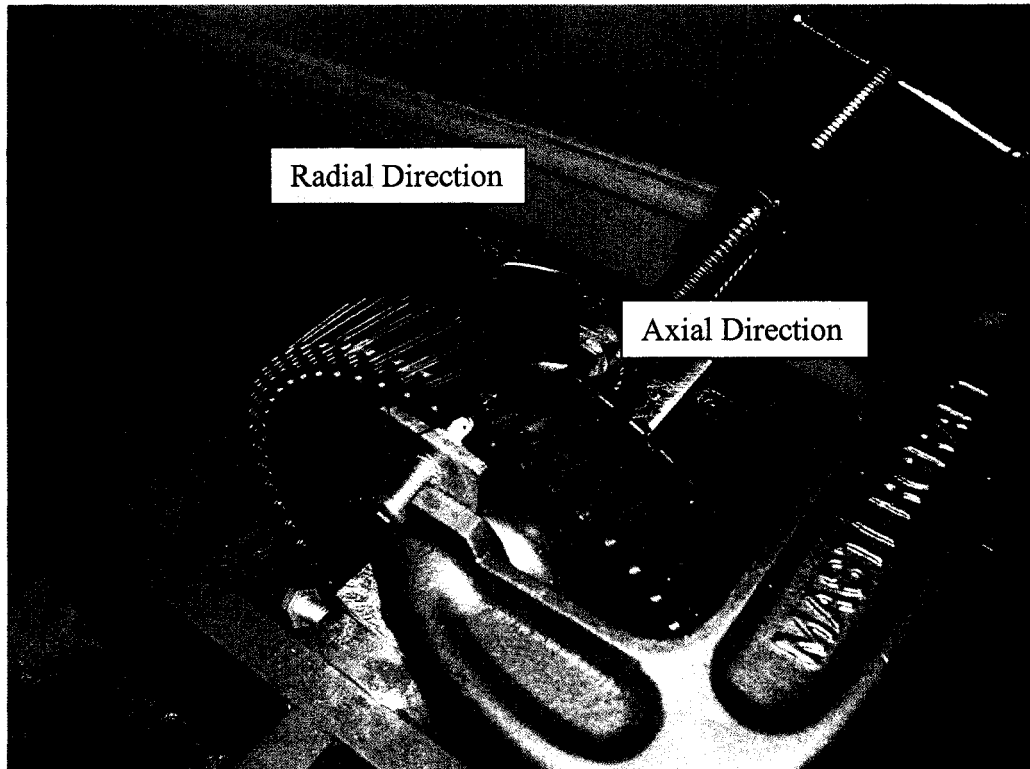
Figure 11   Experimental test mount simulation of centrifugal force

To recreate the same boundary conditions in the FEM model, the centrifugal force was removed and replaced by a displacement of 0.1 inch (approximate value) in the axial and radial directions based on the conical shape at which the screws are inserted (Figure 12).
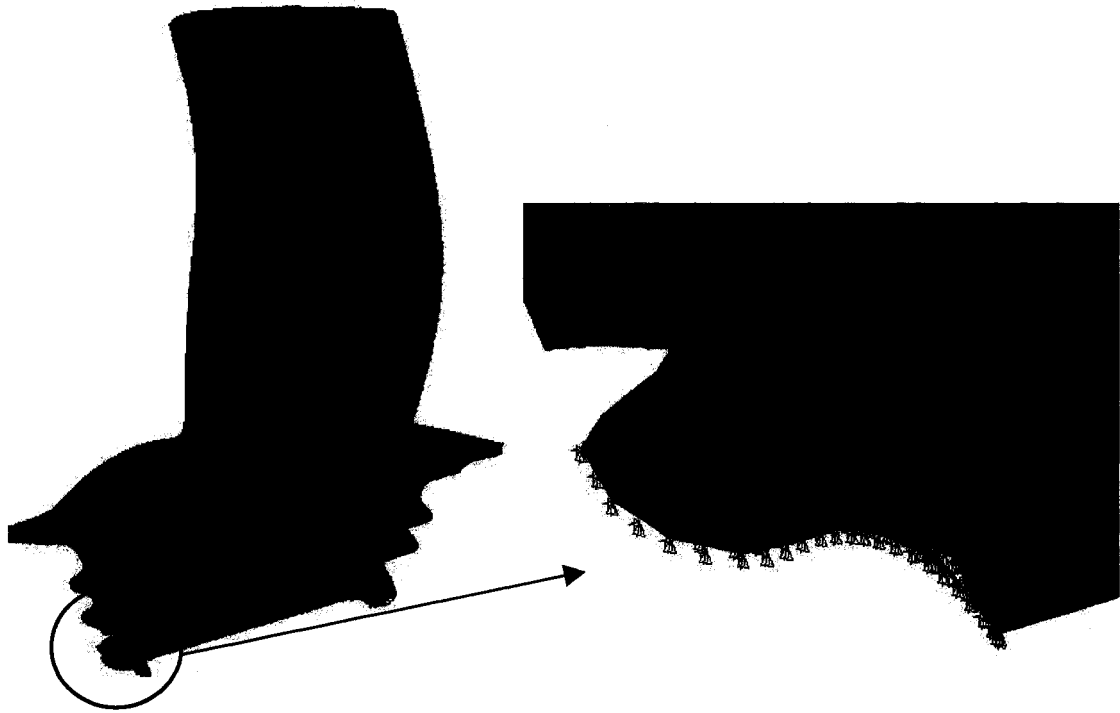
Figure 12   FEM model experimental boundary conditions

5.2   Response Signature Recording

When performing modal testing, usually a hammer is used to excite the component while an accelerometer is used to register the response signal of the component. This is not a concern when the component weighs significantly more than the accelerometer. In this case, the weight on the CT blade is less than ten (10) times the weight of the smallest accelerometer. Therefore, to avoid the shift in frequency due to weight of the accelerometer, a PolyTec laser vibrometer will be used instead (Figure 13).
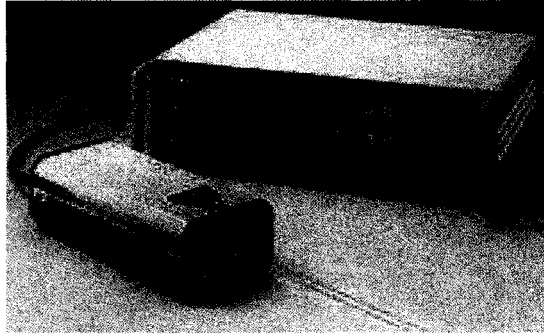
Figure 13   PolyTec Laser Vibrometer

The laser vibrometer will record nine (9) different points of the blade's airfoil so that a mode shape can be created using all the signals (Figure 14).
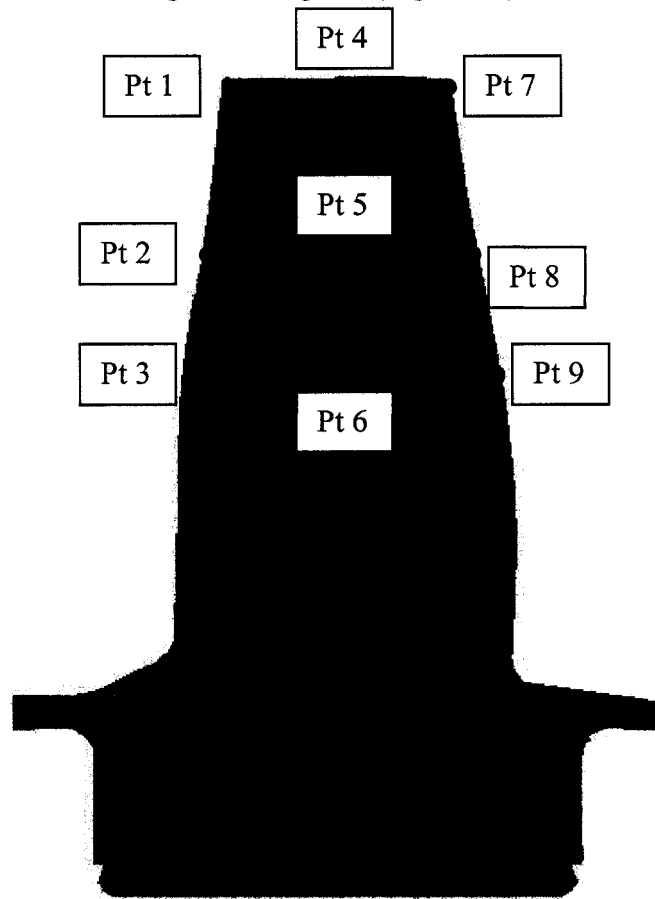
Figure 14   Blade signal recording locations

5.3 Excitation

To excite the CT blade, instead of a typical hammer, a high frequency speaker, JBL Professional Series Model No. 2425 coupled to a Model No. 2306 horn will be used (Figure 15).
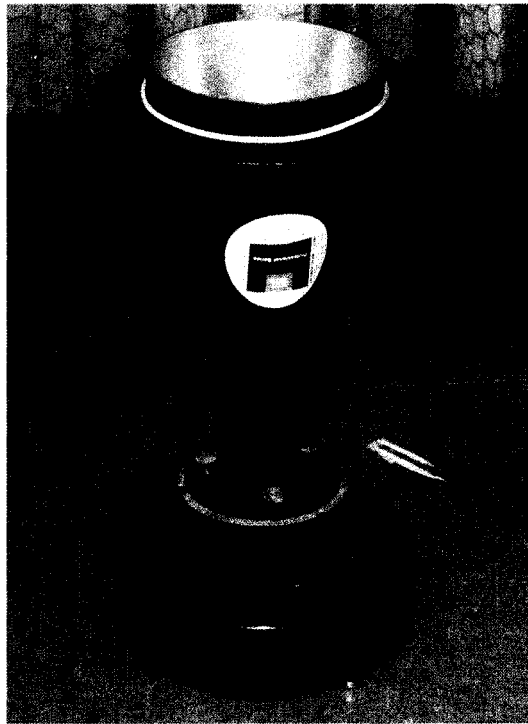
Figure 15   JBL Professional Series Model No. 2425 High Frequency Speaker coupled to Model No. 2306 Horn

A frequency generator is used to create the sine sweep from 2000 to 20000 Hz. The frequency generator is connected through a mixer Mackie Micro Series 1202-VLZ and then to an amplifier from TOA Corporation Dual Power Amplifier Model: IP-300D from which its output is connected to the JBL high frequency speaker.

5.4 Data Acquisition

The data acquisition system used is a Zonic Medallion, 8 channels 0 to 20 kHz. The velocity output of the vibrometer is directly connected to one of the channels. The output of the speaker is recorded through a sensitive microphone placed next to the blade and connected to another channel. The data acquisition parameters used during the experimental testing will give the best frequency resolution throughout the 2000 to 20000 Hz frequency range. The data acquisition program generates a Frequency Response Function (F.R.F.) by dividing the laser vibrometer signal by the microphone signal. The real and imaginary parts of the F.R.F will be used to determine the natural frequencies of the blade and the associated mode shape. The results are presented in section 7.3.

CHAPTER 6

VIBRATORY STRESS ANALYTICAL PREDICTION

Turbine blades are subjected to vibratory stresses due to unsteady flow in the gas path. The unsteadiness of the flow creates different load paths on the blade airfoil and coupled with the natural mode shape of the blade at that exact frequency, resonance occurs at which, high vibratory stresses are associated. This problematic is also known as "aero elasticity". Many sources of unsteady flow exist in turbomachines, such as:

> ➢ Blade / Vane wakes
> ➢ Blade / Vane potential fields
> ➢ Tip vortices
> ➢ End wall vortices

Most unsteady flows are circumferentially periodic and an integer multiples of rotor speed.

To predict turbine blade vibratory stresses analytically, both FEM modal solution and CFD solution at the resonance speed have to be coupled [2]. The modal solution was presented in section 4.2. The CFD solution is not presented or studied in this research but in a condensed form; an Euler CFD solution is performed to determine the steady part of the flow and to calculate the aerodynamic damping. The unsteady part of the flow is determined using a Navier-Stokes CFD solution where a turbulence model is introduced. Both steady and unsteady (vs. time) solutions are required to predict the aerodynamic load on the turbine blade.

6.1 FLARES Analytical Tool

To couple the aerodynamic solution to the mechanical model, an analytical tool called "FLutter And REsonance Stress Prediction System" (FLARES) has been developed by Pratt & Whitney East Hartford [2]. The following description of the code has been derived from the FLARES technical manual.

For FLARES to determine the vibratory stresses, it has to solve the following turbomachinery aeromechanics equation:

$$[M]\{\ddot{u}\} + [C(\ddot{u},\dot{u},u,\Omega)]\{\dot{u}\} + [K(u,\Omega)]\{u\} = \{P(\ddot{u},\dot{u},u,t)\} + \{F(u,\Omega)\} \tag{6.1}$$

[M]   Structural mass matrix

[C]   Structural damping matrix

[K]   Geometrically nonlinear stiffness matrix including centrifugal stiffness and softening

{F}   Nonlinear centrifugal force vector

{u}   Structural position vector

Ω Engine Rotational Speed

t   Time (sec)

For the aerodynamic part, equation 6.1 can be solved with the steady state equation at the blade running position and steady stress. The perturbation assumption plus the separation of motion and gust loads are solved with the following equations:

$$\{u\} = \{\overline{u}\} + \{\tilde{u}(t)\} \tag{6.2}$$

$$\{P(\ddot{u},\dot{u},u,t)\} = \{\overline{P}(\overline{u})\} + \{\tilde{P}_M(\tilde{u},\overline{u})\} + \{\tilde{P}_G(\overline{u},t)\} \tag{6.3}$$

$\{\overline{u}\}$ Time-averaged position

$\{\tilde{u}(t)\}$ Time dependent displacement

$\{\overline{P}(\overline{u})\}$ Time average aerodynamic forces

$\left\{\widetilde{P}_M(\widetilde{u},\overline{u})\right\}$ Airfoil vibratory motion dependent forces

$\left\{\widetilde{P}_G(\overline{u},t)\right\}$ Unsteady aerodynamic forces caused by "gust".

The aeroelastic equation is separated into the independent part of the airfoil vibratory motion:

$$[K(\overline{u},\Omega)]\{\overline{u}\} = \{P(\overline{u})\} + \{F(\overline{u},\Omega)\} \qquad (6.4)$$

$[K(\overline{u},\Omega)]$ Geometrically nonlinear stiffness matrix

$\{F(\overline{u},\Omega)\}$ Nonlinear centrifugal force

Equation 6.4 is iteratively solved for $\{\overline{u}\}$.

The turbine blade natural frequency and mode shape for the specific resonance speed is solved while assuming an airfoil simple harmonic motion and in a vacuum structural dynamics:

$$\{\widetilde{u}(t)\} = \{\phi\}e^{iwt} \qquad (6.5)$$

$$[[K(\overline{u},\Omega)] - \omega^2[M]]\{\phi\} = 0 \qquad (6.6)$$

$\{\varphi\}$ Mode shape, eigenvector

ω Natural frequency, eigenvalue

The assumption of the airfoil simple harmonic motion is based on PWC's experience where the HPT or CT blade modes are not coupled. The mode shape and natural frequency are solved using ANSYS®.

The turbine blade vibratory motion is a linear combination of orthogonal mode shapes:

$$\{\widetilde{u}\} = [\Phi]\{q\} \qquad (6.7)$$

The motion dependent loads are a sum of loads from orthogonal mode shapes:

$$\{P_M\} = [P(\Phi)]\{q\} \qquad (6.8)$$

$[\Phi]$ Normal modes

$\{q\}$ Normal or modal coordinates

$[P(\Phi)]$ Aerodynamic forces from the normal modes.

If substituted in the aeroelastic equation and premultiplied by $[\Phi]^T$, the orthogonality of $[\Phi]^T$ is creating an advantage and the assumed structural damping is represented by ζ:

$$[I]\{\ddot{q}\}+[2\zeta_j\omega_j]\{\dot{q}\}+[\omega_j^2]\{q\}-[Q]\{q\}=\{L(\omega)\} \qquad (6.9)$$

While simple harmonic motion is assumed: $\{q\}=\{q_0\}e^{iwt}$

$$\left[\omega^2\left[\frac{\omega_j^2}{\omega^2}-1+2i\zeta_j\frac{\omega_j}{\omega}\right]-[Q(\omega)]\right]\{q_0\}=\{L(\omega)\} \qquad (6.10)$$

$[Q(\omega)]=[\Phi]^T[P(\Phi)]$: the generalized airfoil motion dependent forces;

$[L(\omega)]=[\Phi]^T[P_G(\omega)]$: the generalized gust dependent model force; $[P_G(\omega)]$ is the Fourier Transform of $[P_G(t)]$.

Therefore, for a single mode:

$$q_0=\frac{L(\omega)}{Im[2i\zeta\omega^2-Q(\omega)]} \qquad (6.11)$$

Knowing the modal coordinates {q}, the physical vibratory displacements and stresses $\{\tilde{u}\}$, can be determined by:

$$\{\tilde{u}\}=[\Phi]\{q\} \qquad (6.12)$$

Practically, the single mode equation can be written this following way:

$$\sigma=F\cdot\sigma_{modal} \qquad (6.13)$$

where:

$$F = \frac{\pi L}{\omega^2 (\delta_{aero} + \delta_{mech})} \qquad (6.14)$$

σ Vibratory stress for a single mode

$\sigma_{\mathrm{mod}\, al}$ Modal vibratory stress for a single mode (given by ANSYS)

F   Modal amplification factor

L   Modal force

δ_{aero} Aerodynamic damping (logarithmic decrement)

δ_{mech} Mechanical damping (logarithmic decrement)

Using the CFD analyses for particular resonance speeds, the modal amplification factor will be determined by FLARES. This factor will then multiply the modal vibratory stress vector in ANSYS® to obtain the analytical predicted turbine blade resonance vibratory stresses. The results are presented in section 7.4.

CHAPTER 7

RESULTS AND DISCUSSION

The first results presented will be on the SGT data reduction performed on High Pressure Turbine Blades of various engines. The following results will show the correlation in natural frequencies and mode shapes obtained for analytical modeling using contact elements versus the results data obtained from the SGT data reduction. The last section will present the results on the correlation between the analytical vibratory stress prediction and the vibratory stress results obtained from the SGT data reduction.

7.1   Strain Gage Test Data Reduction Results

This section will present the results from the SGT data reduction performed on the PWC Engine 1, PWC Engine 2 and PWC Engine 3 engines. The results will be presented in tables, one for each engine and in three main sections: resonance results, damping extraction results and stress results.

7.1.1   Resonance results

The resonance results presented in the following tables represent only the highest peak strain values for each mode and strain gage location during the data reduction. Since only the maximum strain values are of concern, only the corresponding run number (Run column) and strain gage location (SG column) are presented. The natural frequency values may differ for different strain gage location since the strain gages are placed on different blades. Turbine blades have little differences between them that would slightly shift the natural frequencies, although the mode and harmonic excitation are the same. In addition, the crystal orientation would create differences in the natural frequency values. The Mode column presents which mode (ex: M2) is in resonance with

which excitation harmonic (ex: 1H for first harmonic). The frequency (Frequency column) and the engine rotating speed (N2 or Ng) associated with the resonance are given. The modes and excitations presented in the following tables are the only ones that were in resonance within the engine speed operating range. The natural frequencies are normalized to the first frequency value of the tables.

Table IV

PWC Engine 1 Resonant Frequencies

Airfoil RPM

Mode	SG	Run	Frequency	N2
M2-1H	3E	8485/1/11	1.0	35222
M4-2H		8485/1/11	1.558	33321
M2-1H	1D	8485/1/11	1.0	35231
M4-2H		8485A/1/11	1.564	33517
M2-1H	12G	8485A/1/11	1.0	35235
M4-2H		8485A/1/11	1.538	32906
M2-1H	5F	8485A/1/11	1.016	35766
M4-2H		8485/1/11	15456	33134
M2-1H	7M	8485A/1/11	1.0	35332
M4-2H		8485A/1/11	1.503	32215

Fixing RPM

Mode	SG	Run	Frequency	N2
M2-1H	8A	8485A/1/11	1.016	35786
M4-2H		8485A/1/11	1.535	32852
M2-1H	9C	8485/1/11	1.006	35456
M4-2H		8485/1/11	1.535	32852

The results for the natural frequencies of the other engine models are presented in APPENDIX 2.

7.1.2 Modal damping extraction results

The total damping values presented below are separated by engine models, modes and harmonic excitations. The total damping values were extracted from the SGT data reduction presented in section 3.2. The curve fitting was performed and the minimum R^2 value was of 0.912. To complete the damping analysis, a correlation has to be done in function on the wetted area of the blade and the excitation harmonic. It is believed that the mechanical damping and the aerodynamical damping is function of the wetted area of the blade. Although, there are many other parameters, which are functions of the damping, it was chosen to observe this particular one. The extracted damping is in the logarithmic decrement form and transformed to zeta form (ration between the damping and the critical damping) form using the following equation:

$$\zeta = \frac{\delta}{\sqrt{\delta^2 + 4\pi^2}} \tag{7.1}$$

Table V

PWC Engine 1 Modal damping

Mode	M2		M3		M4	
Excitation	2H		2H		2H	
Harmonic	2nd		2nd		2nd	
Damping	Dec. Log.	Zeta (%)	Dec. Log.	Zeta (%)	Dec. Log.	Zeta (%)
Data	0.0223	0.355%	0.0121	0.193%	0.0163	0.259%
	0.0240	0.382%	0.0128	0.204%	0.0186	0.296%
	0.0240	0.382%			0.0153	0.243%
	0.0242	0.385%			0.0133	0.212%
	0.0304	0.484%			0.0194	0.309%
Average	0.0250	0.398%	0.0125	0.198%	0.0164	0.264%
Q value	125.6		252.5		189.4	
Variance	9.77E-06	2.48E-07	2.45E-07	6.21E-09	1.79E-05	1.54E-07

The results for the modal damping of the other engine models are presented in APPENDIX 3.

The damping correlation was made in regards to the excitation harmonic and the blade airfoil wetted area (Figure 16).
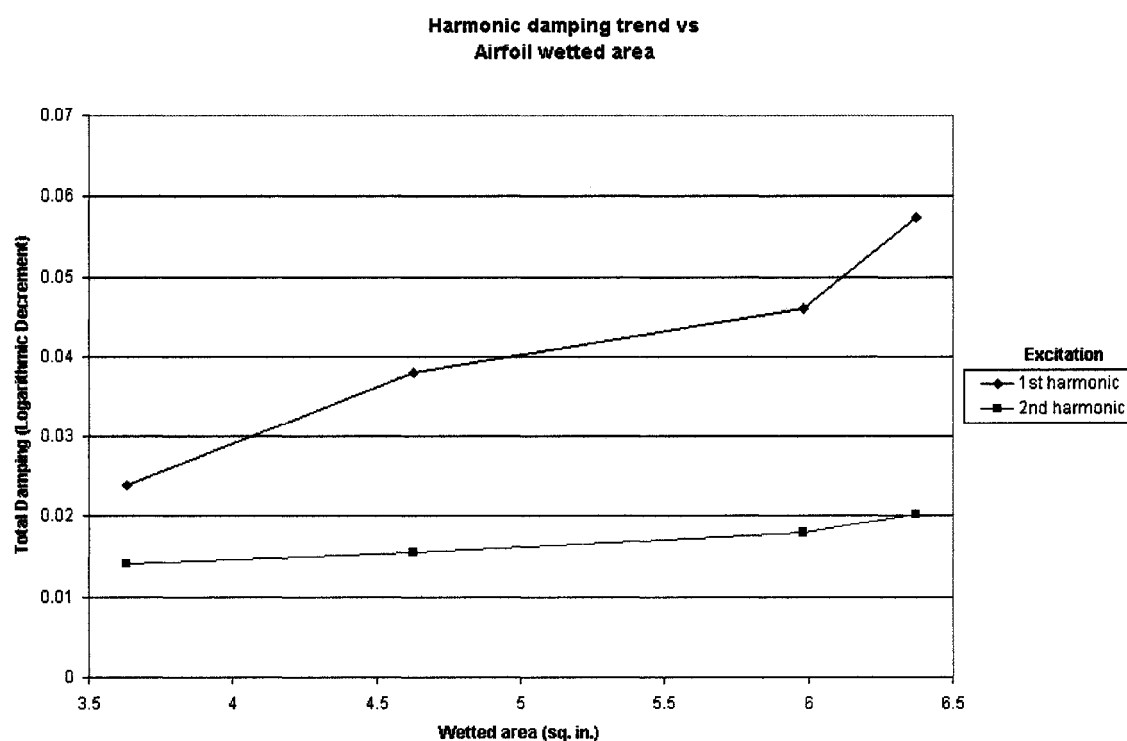
Figure 16   Harmonic damping trend vs. Airfoil wetted area

The correlation between the total damping and the blade airfoil wetted area show that they are linear with each other. The higher the wetted area, the higher the total damping value will be. Furthermore, the 2nd harmonic excitation total damping is much lower than the 1st harmonic excitation. This would explain why we see such high vibratory stresses for 2nd harmonic excitation.

7.1.3 Experimental vibratory stress results

The following tables present the stress results from the SGT data reduction of the PWC Engine 1, PWC Engine 2 and PWC Engine 3. The waterfall strain (WF strain) peak values are obtained directly from the resonance point of the waterfall plot (Figure 4). The overall strain (OA strain) is obtained by the square root sum of the strain values of the whole frequency range for a given resonance speed. The engine order strain (EO strain) is the peak value obtained from the whole engine order excitation speed and within a certain frequency band. All the strain values are given in micro strain (10^{-6}) format. The blade strain gage location metal temperature (T metal) was obtained from a steady thermal analysis. The Young's modulus (E) was obtained from the material properties of each blade at the given metal temperature and strain gage orientation.

Table VI

PWC Engine 1 Vibratory Stress

E6211B6

Airfoil			RPM	ksi	ksi	ksi
Mode	**SG**	**Frequency**	**N2**	**WF stress**	**OA stress**	**EO stress**
M2-1H	3E	1.0	35222	0.6304	1.2555	0.1799
M4-2H		1.558	33321	11.7580	11.9439	11.8257
M2-1H	1D	1.0	35231	2.6215	3.0175	0.2644
M4-2H		1.564	33517	1.0654	1.6468	3.0482
M2-1H	12G	1.0	35235	7.8369	8.5780	6.3823
M4-2H		1.538	32906	5.2755	5.8280	13.4422
M2-1H	5F	1.016	35766	1.5157	3.3161	2.5611
M4-2H		15456	33134	10.9549	11.2905	0.0000
M2-1H	7M	1.0	35332	4.7775	6.3161	19.2286
M4-2H		1.503	32215	2.4487	4.6595	13.7954

Table V (continued)

Fixing		Hz	RPM	ksi	ksi	ksi
Mode	**SG**	**Frequency**	**N2**	**WF stress**	**OA stress**	**EO stress**
M2-1H	8A	1.016	35786	0.9460	2.1165	2.9464
M4-2H		1.535	32852	0.6582	1.6300	1.3487
M2-1H	9C	1.006	35456	0.7692	2.1214	0.3901
M4-2H		1.535	32852	2.0652	2.5273	2.0789

Due to data storage discrepancies, the stress values for the PWC Engine 2 HPT blade could not be found. This was remedied to be best accuracy by using the stress value from the certification reports.

The results for the vibratory stress of the other engine models are presented in APPENDIX 4.

7.1.4   Discussion on the strain gage data reduction results

The resonances were identified for each CT or HPT blade of various engines. Using the resonance points, the modal damping was extracted.

The modal damping values were presented in the logarithmic decrement form and a zeta form for each engine CT or HPT blades. It was noticed that the higher the harmonic excitation, the lower the total modal damping value would be. Furthermore, the smaller the wetted volume of the blade is, the lower the total modal damping. This is an important fact, especially when these damping values will be used for new engines development with similar blade sizes and shapes. The variance for some engine was very good while others seem to have high difference for the same mode. This can be explained with the quality of the SGT data. If the signal is noisy or the modes are coupled, it is difficult to fit a SDOF curve on the test signal.

The strain values at each identified resonance were extracted. By multiplying the strain with the Young's Modulus, which is function of the metal temperature and orientation of the strain gage, the vibratory stress values at each resonance were found. The values of stress seem to be consistent in regards to different modes and harmonic excitations. Since these values were obtained experimentally, it is assumed that they can be used for analytical comparison.

7.2   Results of the Updated Boundary Conditions Analyses

The initial study presented in the primary results and the convergence study were performed on the PWC Engine 1 HPT blade. This blade represents most of the blades analyzed in this study and therefore, the findings can be extrapolated to the other engine models. The analytical results of all the CT or HPT blades studied are also presented.

7.2.1   Comparison between the current and the new analyses

The natural frequencies obtained from the new analysis with contact elements compared to the strain gage values were found to be in good agreement. The natural frequencies computed for modes 1 and 2 were found to have an average error range of 5 to 8% while modes 3 and 4 were found to have an average error range of 0 to 2%. The mode shapes were found to be identical between the current and the new analyses (using same displacement scale) (Figure 17 & 18).
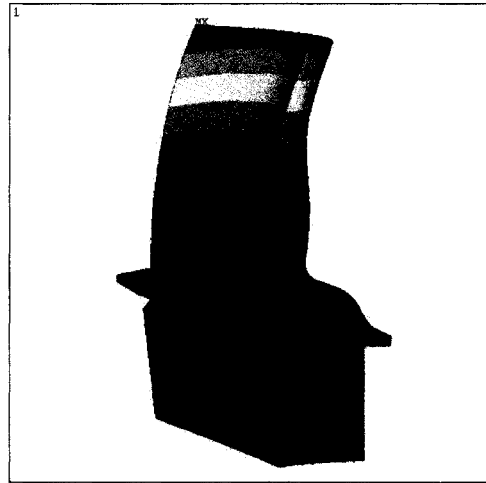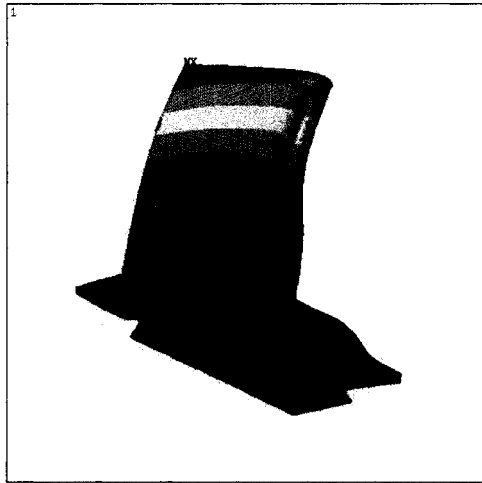
Figure 17   Current analysis mode shape   Figure 18   New analysis mode shape

Furthermore, the stress levels in the fir-tree area were compared of the current (see Figure 8) and the new analyses using contact elements (Figure 19) were compared.
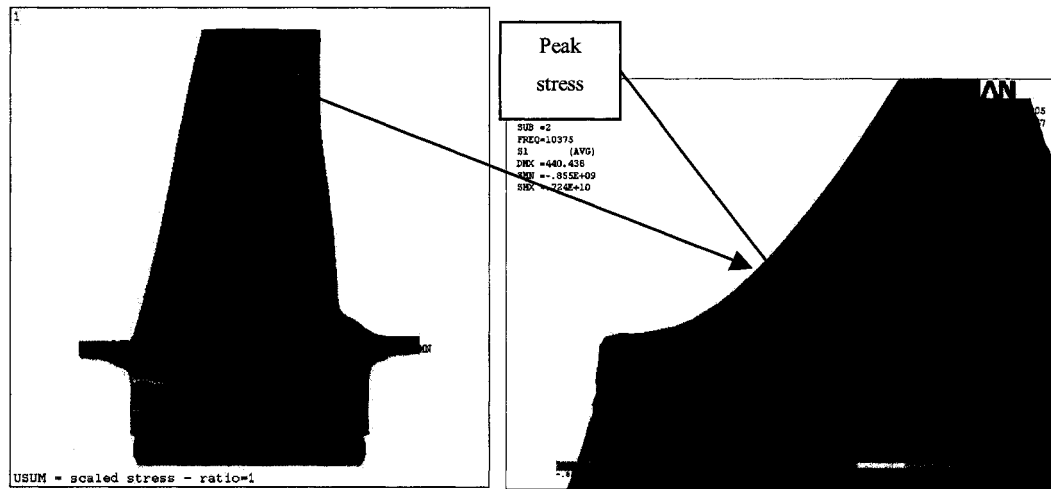
Figure 19   Blade stress in the fir-tree area (Inside the airfoil's cooling pocket)

The stress level in the fir-tree area for the new analysis was found to be lower by a factor of approximately 40% compared to the current analysis. It can therefore be assumed that the new analysis with contact elements will predict stress levels with more accuracy than

will the current analysis. Finally, it was confirmed that the contact face was enlarged by 5% during the pre-stress static analysis (Figure 20).
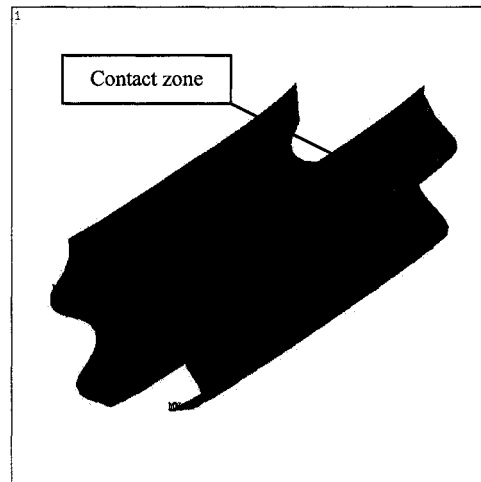
Figure 20   Contact face width

This result proves that the blocked contact face does not reflect the phenomenon, and therefore should not be used in such analyses.

7.2.2   Convergence study

A study was performed to determine the contact element parameter values, which would yield the best convergence results. This study was performed on multiple models of blades to ensure reproducibility for the next designs. The first parameter studied was the friction coefficient (MU) (Figure 21).
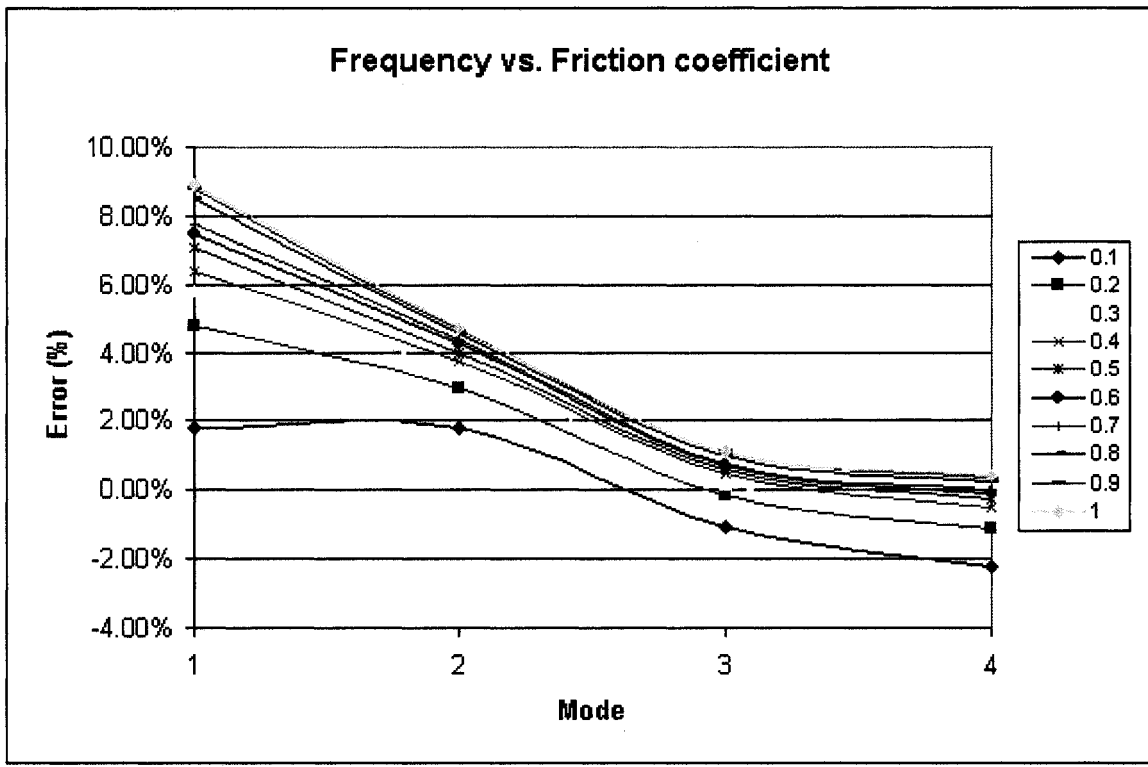
Figure 21   Frequency error vs. friction coefficient

A convergence was found between the values 0.9 to 1. This showed that the model was stable, and that convergence could be achieved. It was noticed that the higher the friction coefficient value, the higher the error for modes 1 and 2, while modes 3 and 4 tended to remain the same. This seems to indicate that mode 1 and 2, i.e. first bending and first torsion, are much more susceptible to sliding friction than the higher order modes (mode 3 and 4), although this phenomenon needs to be further evaluated. Therefore, there is an optimum friction coefficient value for each mode. In this case, for mode 1 and 2, a friction coefficient value between 0 and 0.1 would minimise the error, while a friction coefficient close 1.0 would minimise the error for mode 3 and 4.

The second parameter studied was the normal contact stiffness factor (FKN) (Figure 22).
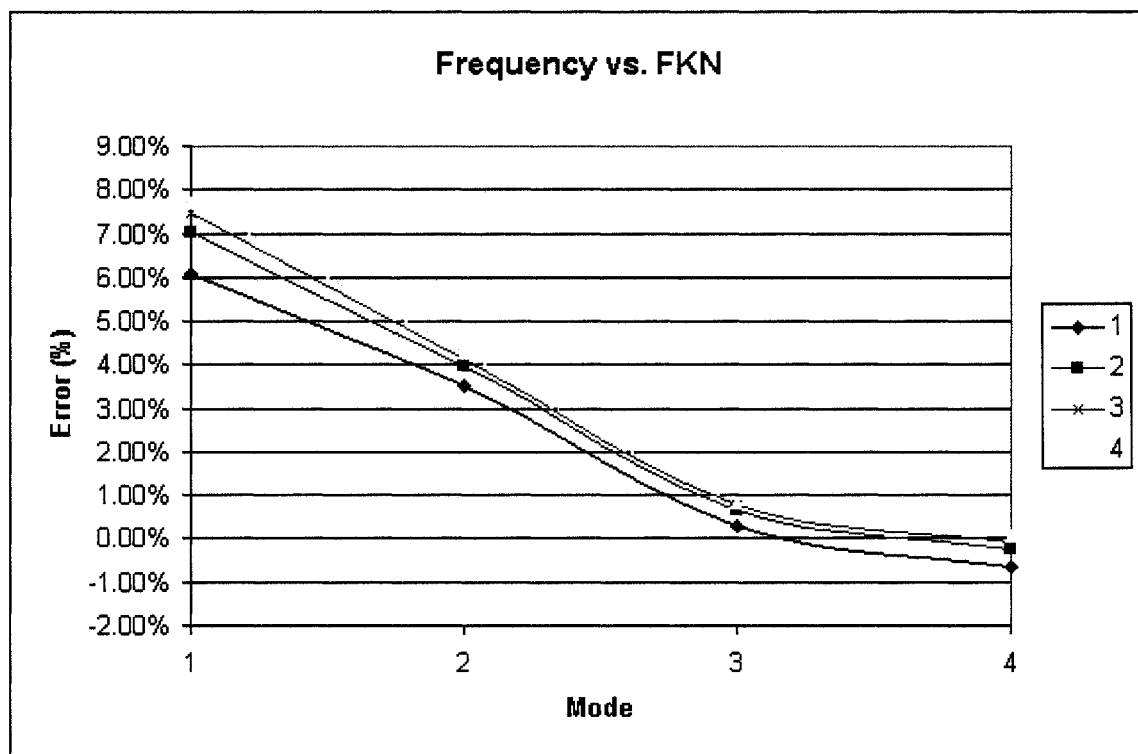
Figure 22   Frequency vs. Normal contact stiffness factor

It was noticed that the error tends to proportional to the normal contact stiffness factor. This indicates that the higher the factor, the less the penetration that occurs and therefore there is an increase in natural frequency. Convergence is achieved when very little or no penetration occurs between the blade and the disc. This phenomenon has to be studied more thoroughly by performing experimental penetration tests.

The third parameter studied was the penetration tolerance factor (Figure 23).
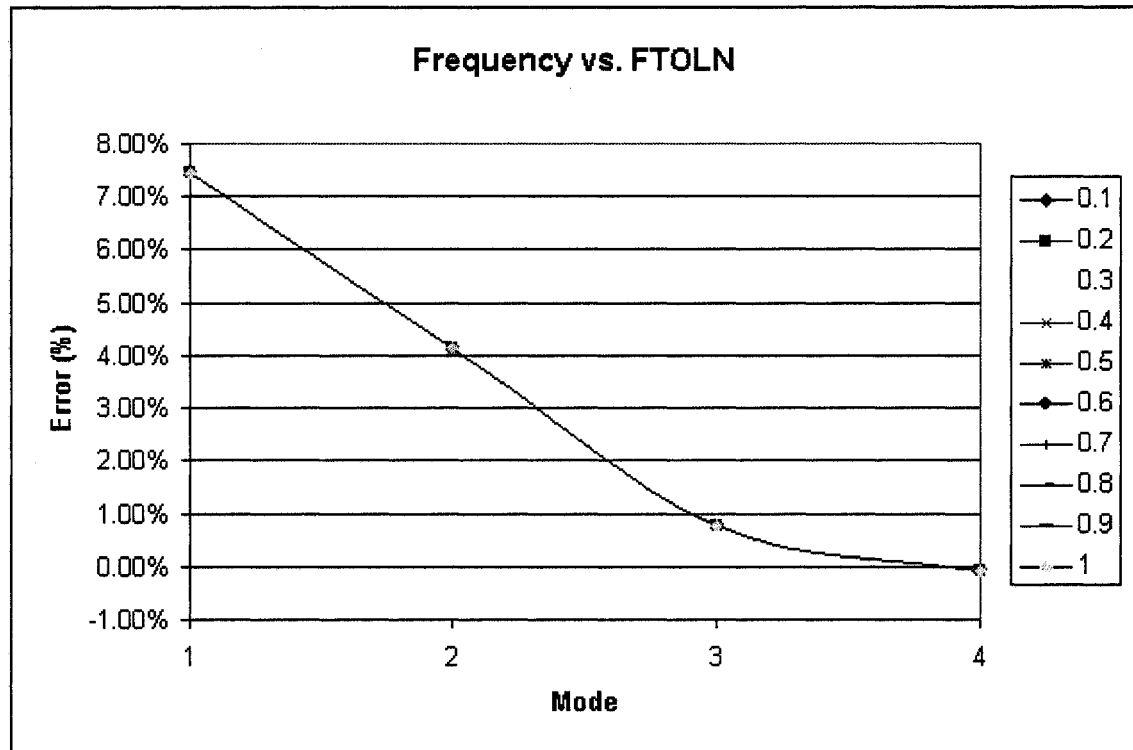
Figure 23   Frequency vs. Penetration tolerance factor

It was observed that the penetration tolerance factor had no effect on natural frequencies. This could be explained by the fact that the analysis predicts a penetration smaller than the allowable value (factor value multiplied by the depth of the underlying solid). Therefore, if the factor is larger than the penetration, the parameter will have no effect on the results. However, the factor cannot be too great or else the model convergence will not be obtained.

The fourth and fifth parameters were studied simultaneously. The ratio between the static and dynamic friction coefficient (FACT) and the slip rate decay coefficient (DC) were varied at the same time during the study (Figure 24).
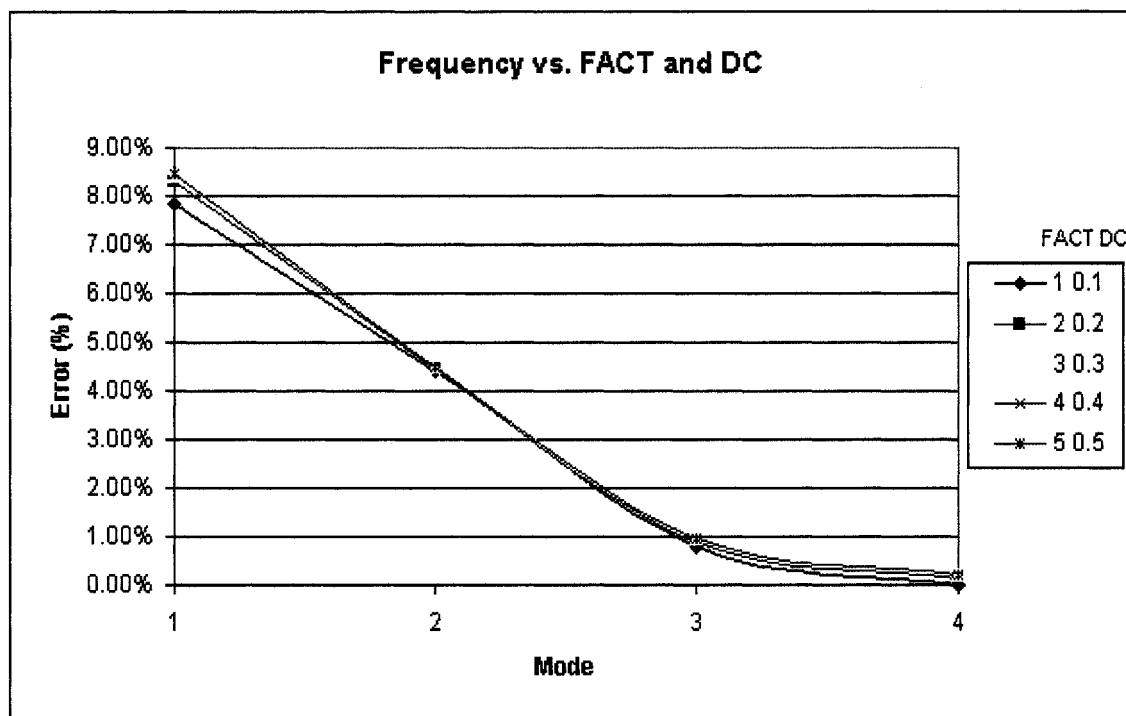
Figure 24   Frequency vs. Ratio between the static and dynamic friction coefficient and the slip rate decay coefficient

The ratio between the static and dynamic friction coefficient and the slip rate decay coefficient were found to have very little effect on the results. This seems to indicate that there is a low slip rate, and thus the parameters have little effect on the friction coefficient.

7.2.3   Analytical results using contact elements modal analysis

The PWC Engine 1 HPT, PWC Engine 2 HPT and PWC Engine 3 CT blades were analyzed using contact elements as boundary conditions between the fixing of the blade and the disc. The natural frequencies of the first four (4) modes were extracted and compared to the average value of the natural frequencies extracted from the strain gage test data. The analyses were performed at either the maximum speed or the resonant speed conditions. The natural frequencies have been normalized to the experimental

value (SGT) of the first mode. Based on the convergence study, the following contact element variable values were used to determine the natural frequencies for each of the engine models blade:

- Dynamic coefficient of friction (MU) = 0.1;

- Normal stiffness factor (FKN) = 1;

- Penetration tolerance factor (FTOLN) = 1;

- Ratio between the static and dynamic coefficient (FACTOR) = 1;

- Slip rate decay coefficient (DC) = 0.1.

7.2.3.1 PWC Engine 1 HPT Blade Natural Frequency Prediction

Table VII

PWC Engine 1 HPT Blade Natural Frequency Comparison @ 35200 RPM

@ 35200 RPM				
Mode	SGT	Std. Dev.	ANSYS	Error
1	1.0	0.27%	1.043	4.35%
2	2.428	0.78%	2.506	3.23%
3	3.237	0.38%	3.360	3.80%
4	3.647	0.72%	3.609	1.04%

52
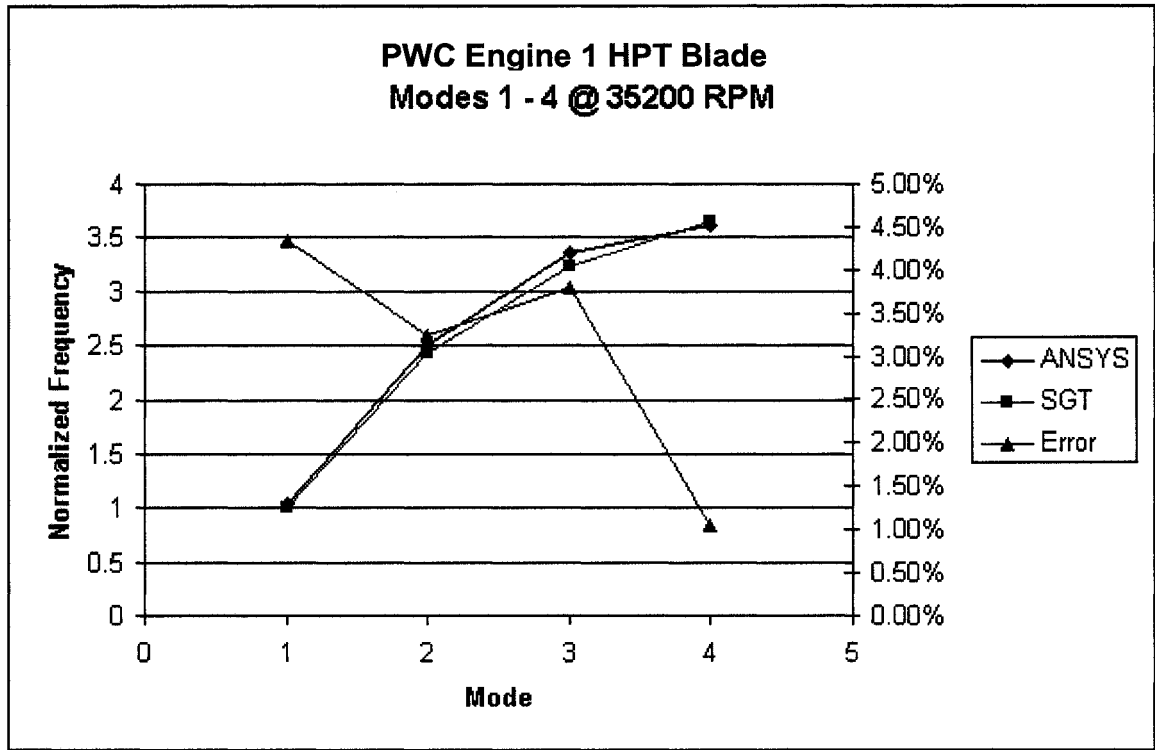
Figure 25   PWC Engine 1 HPT Blade Natural Frequency Comparison @ 35200 RPM

Table VIII

PWC Engine 1 HPT Blade Natural Frequency Comparison @ 33000 RPM

@ 33000 RPM				
Mode	SGT	Std. Dev.	ANSYS	Error
1	1.0	1.35%	1.050	4.98%
2	2.405	0.62%	2.479	3.08%
3	3.283	1.11%	3.415	4.01%
4	3.683	1.28%	3.679	0.13%
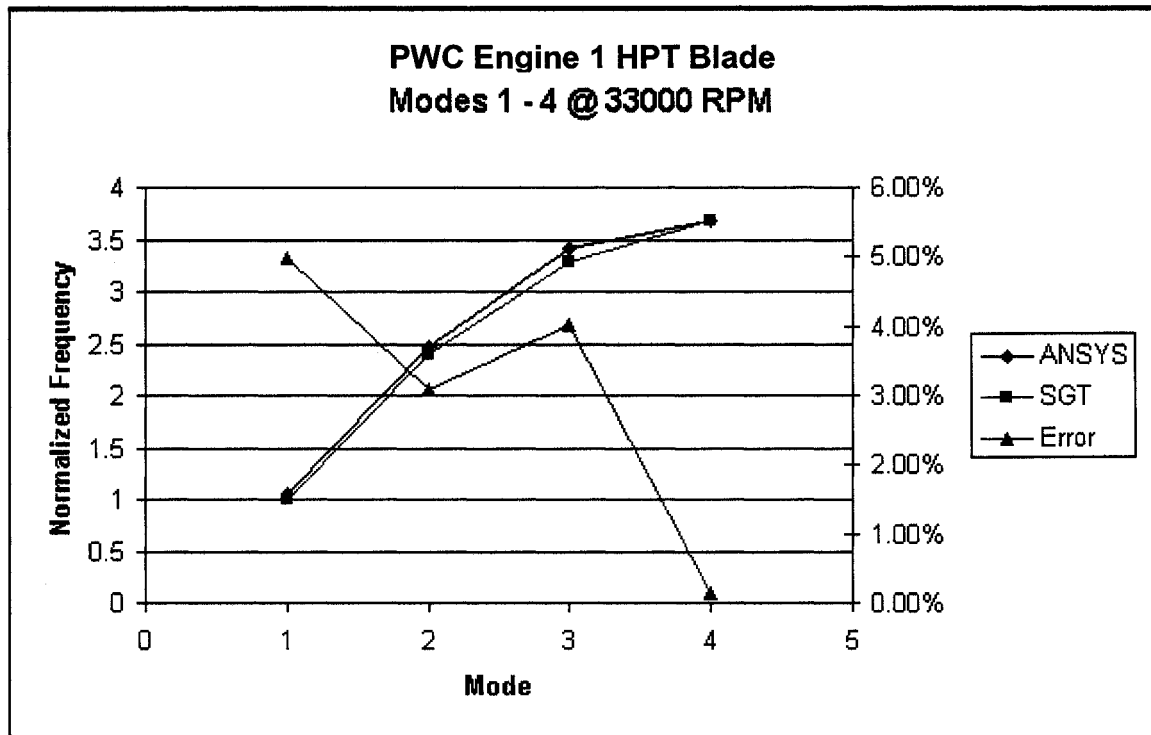
Figure 26   PWC Engine 1 HPT Blade Natural Frequency Comparison @ 33000 RPM

The correlation between the natural frequencies on the analytical solution and the SGT data was within 5% error margin. It was determined that the analytical solution overestimated the first two modes while underestimated the third and fourth modes. The differences can be explained in the geometry used for the analytical compared to the one used during the SGT.

7.2.3.2 PWC Engine 2 HPT Blade Natural Frequency Prediction

Table IX

PWC Engine 2 HPT Blade Natural Frequency Comparison @ 33289 RPM

@ 33289 RPM				
Mode	SGT	Std. Dev.	ANSYS	Error
1	1.0	1.20%	0.956	4.38%
2	2.317	0.17%	2.286	1.37%
3	2.8	7.86%	2.879	2.83%
4	3.8	0.80%	3.675	3.29%
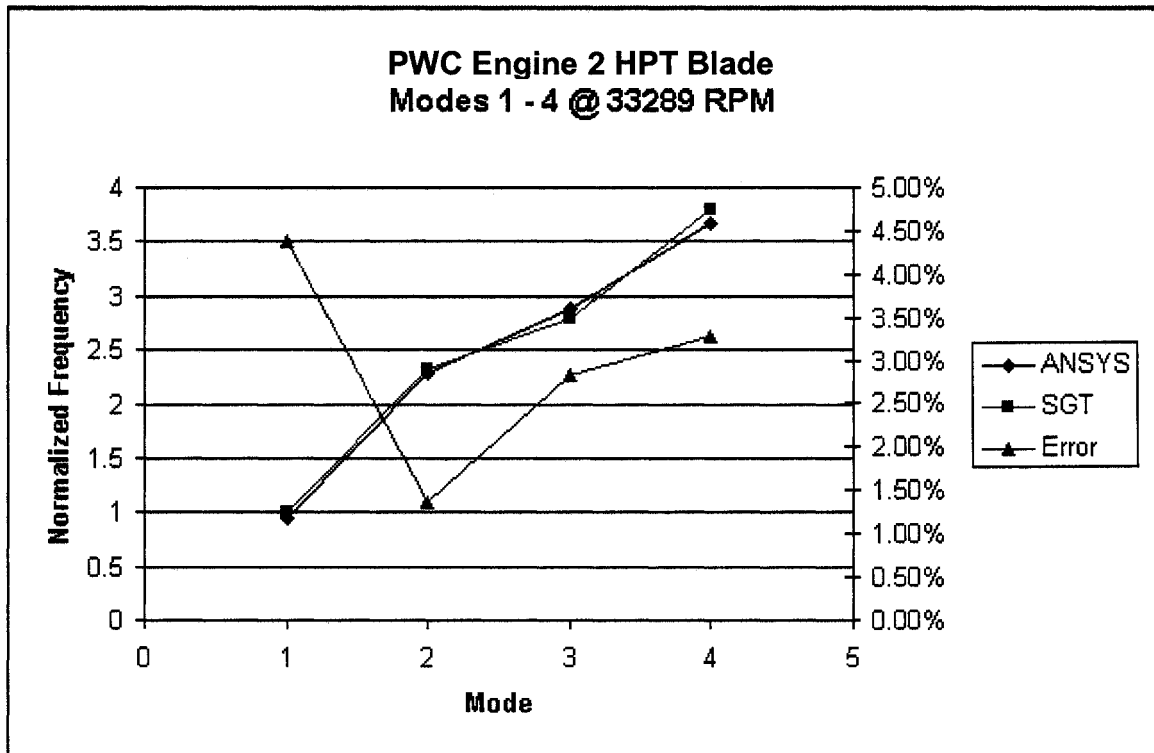
Figure 27   PWC Engine 2 HPT Blade Natural Frequency Comparison @ 33289 RPM

Table X

PWC Engine 2 HPT Blade Natural Frequency Comparison @ 30000 RPM

@ 30000 RPM				
Mode	SGT	Std. Dev.	ANSYS	Error
1	1.0	3.0%	0.962	3.85%
2	2.440	4.47%	2.404	1.48%
3	2.837	1.18%	2.912	2.65%
4	3.821	2.08%	3.678	3.74%
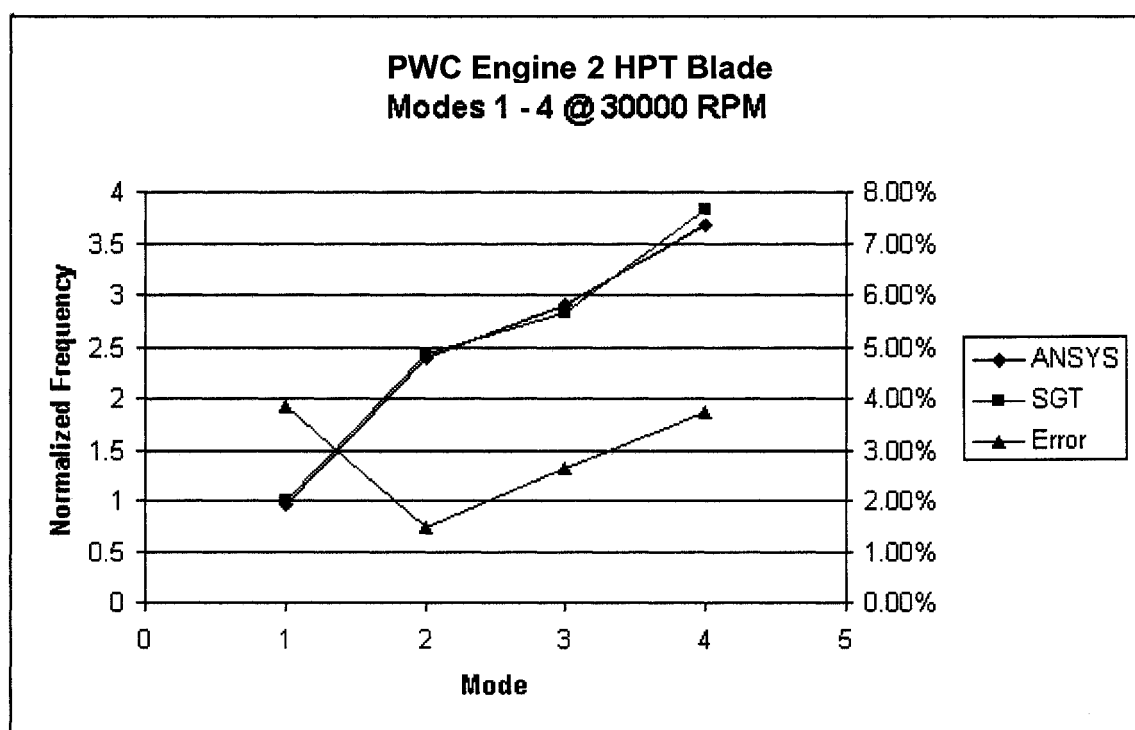
Figure 28   PWC Engine 2 HPT Blade Natural Frequency Comparison @ 30000 RPM

The correlation between the natural frequencies on the analytical solution and the SGT data was within 5% error margin. It was determined that the analytical solution overestimated the first mode only while underestimated the second, third and fourth

modes. The differences can be explained in the geometry used for the analytical compared to the one used during the SGT. Also, a higher dynamic coefficient of friction could be used to increase the natural frequencies determined by the modal analysis.

7.2.3.3 PWC Engine 3 CT Blade Natural Frequency Prediction

Table XI

PWC Engine 3 CT Blade Natural Frequency Comparison @ 43000 RPM

@ 43000 RPM				
Mode	SGT	Std. Dev.	ANSYS	Error
1	1.0	2.36%	0.993	0.65%
2	2.164	0.31%	2.255	4.16%
3	2.799	2.96%	2.931	4.74%
4	3.214	0.79%	3.204	0.29%
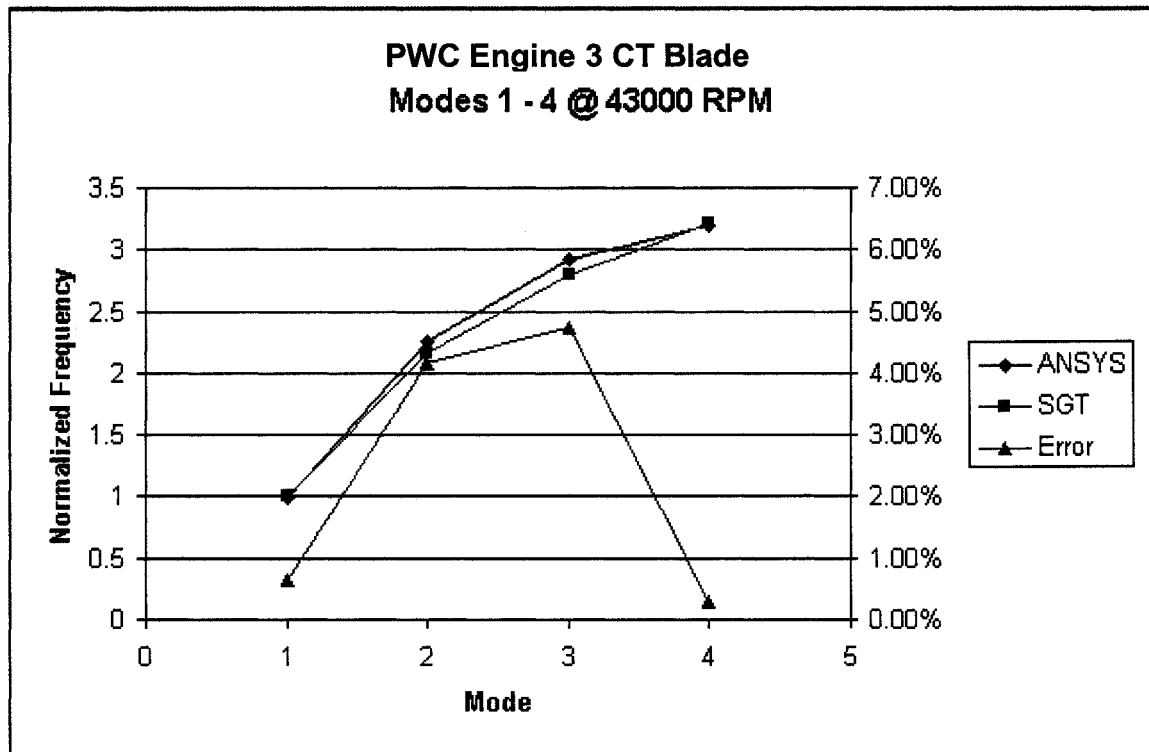
Figure 29   PWC Engine 3 CT Blade Natural Frequency Comparison @ 43000 RPM

Table XII

PWC Engine 3 CT Blade Natural Frequency Comparison @ 36000 RPM

@ 36000 RPM				
Mode	SGT	Std. Dev.	ANSYS	Error
1	1.0	0.90%	1.005	0.54%
2	2.231	1.79%	2.331	4.48%
3	2.854	7.25%	2.994	4.88%
4	3.266	0.25%	3.325	1.81%
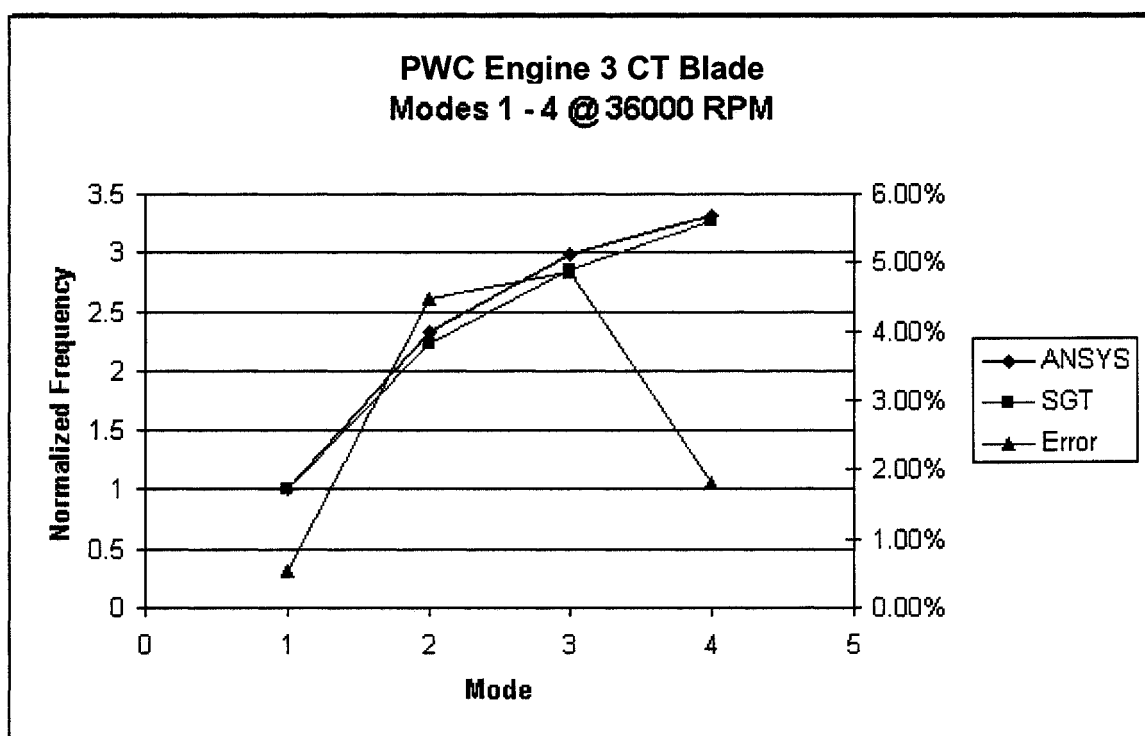
Figure 30   PWC Engine 3 CT Blade Natural Frequency Comparison @ 36000 RPM

The correlation between the natural frequencies on the analytical solution and the SGT data was within 5% error margin. It was determined that the analytical solution overestimated the second mode only while underestimated the first, third and fourth

modes. The differences can be explained in the geometry used for the analytical compared to the one used during the SGT.

7.3 Experimental Tests Results

The experimental testing was not performed with great success. The main deficiency was the excitable frequency range performed by the high-frequency speaker. The JBL Professional Series Model No. 2425 speaker coupled to a Model No. 2306 horn was only able to excite a frequency range from 3500 to 8000 Hz. The excited frequency range was determined by plotting the frequency response of the microphone during the testing period (Figure 31).
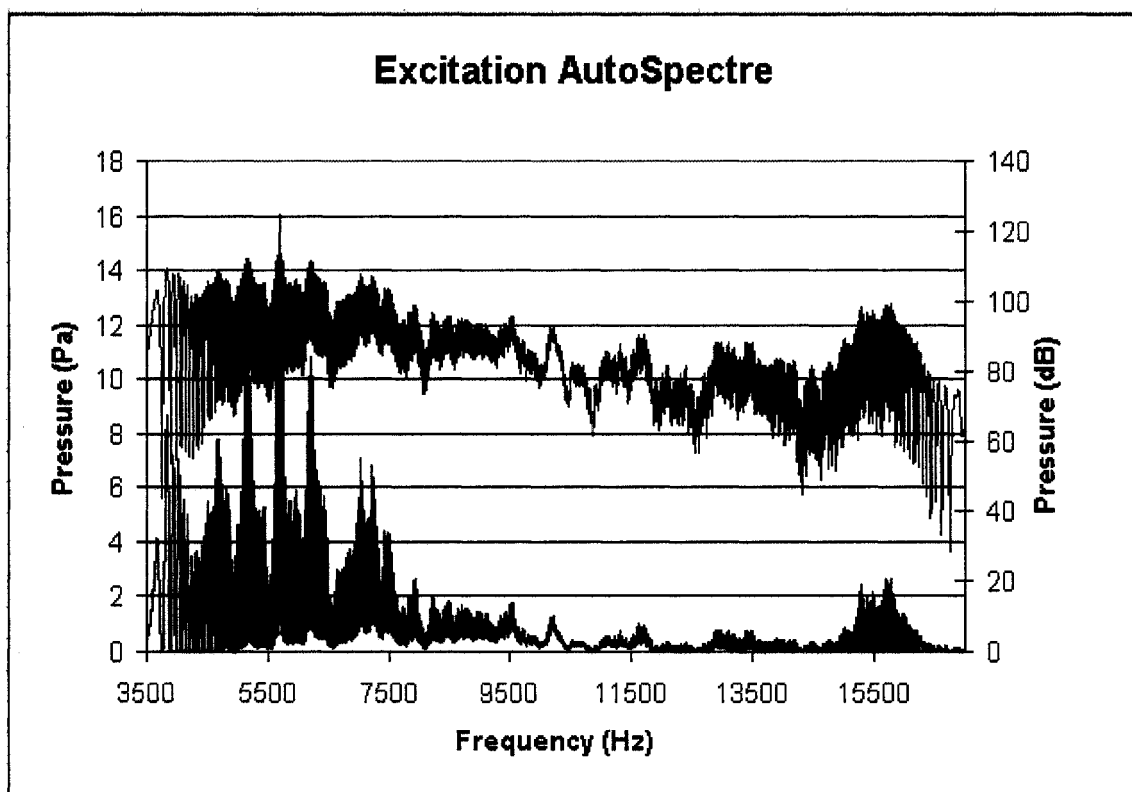
Figure 31 Excitation Autospectrum for excited frequency range

The FEM analysis showed the 4th mode of the Blade used for testing had a natural frequency of 16638 Hz, which is more than double the excited frequency range. Therefore, the results for the 2nd, 3rd and 4th modes will be very questionable. Furthermore, the coherence signal showed weaknesses at multiple frequencies due to the lack excited frequency range.
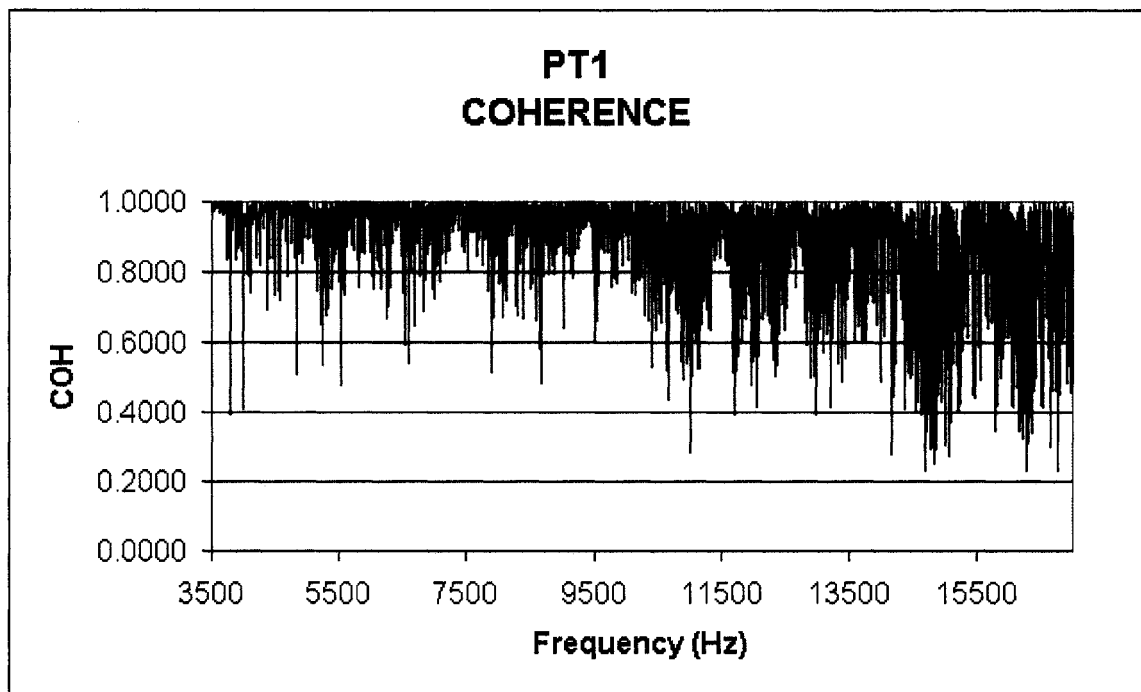
Figure 32   Example of a Coherence signal

To determine the mode shape and damping for each mode, the values (positive or negative) from the F.R.F real signal are taken for each location and natural frequency (Figure 33).
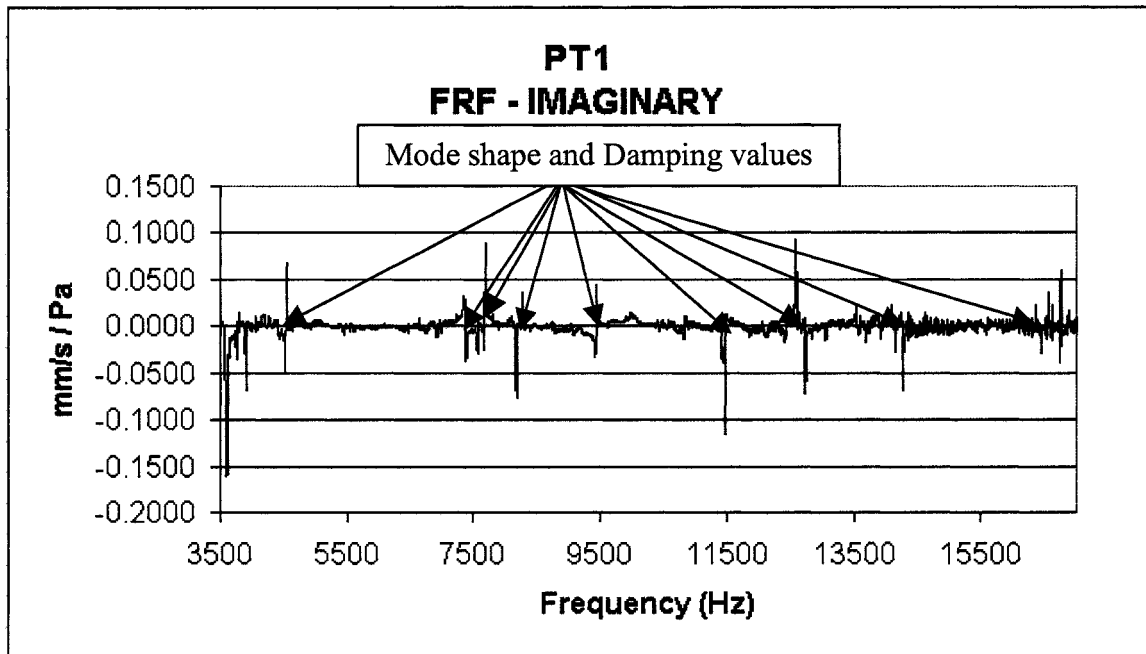
Figure 33   Example F.R.F. signal Imaginary part for mode shape and damping
determination

The natural frequencies were determined by finding the intersection between the F.R.F.

signal imaginary part and the null axis for every location (Figure 34).
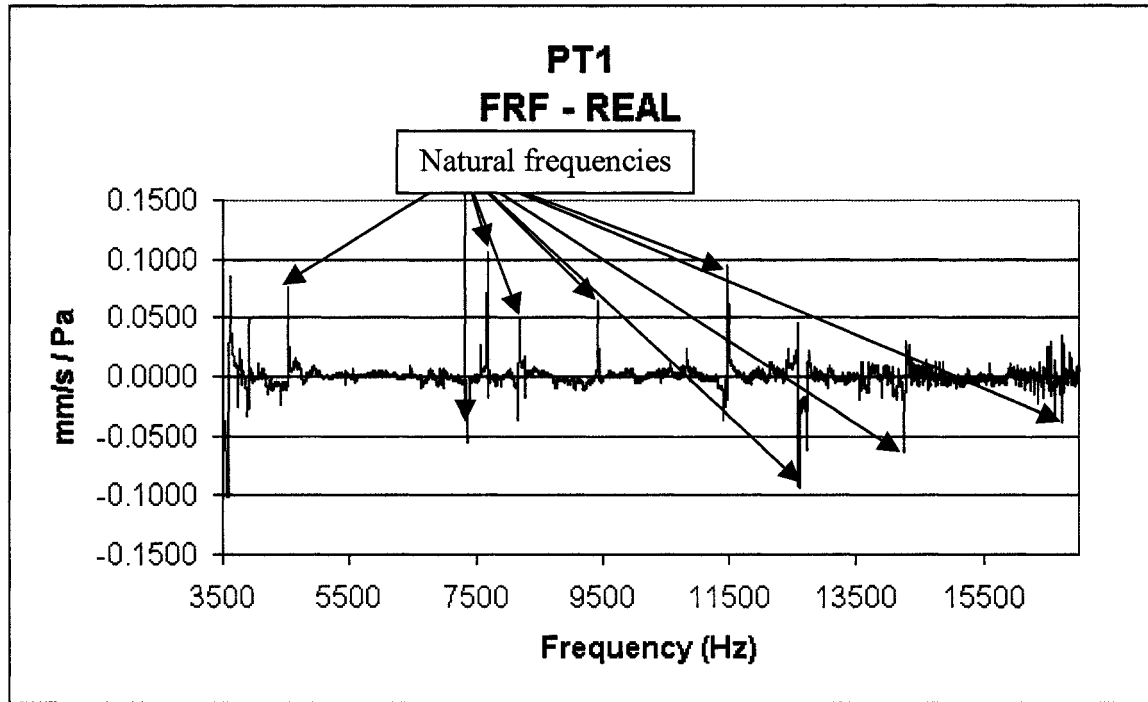
Figure 34   Example F.R.F. signal Real part for natural frequency determination

To extract the damping for each mode, the imaginary part of the signal is used since the F.R.F is in velocity over force (mobility). With the imaginary part of the signal, the two frequencies limiting the bandwidth of the resonance can be determined (w_1 and w_2). With the real part of the signal, the natural frequency of the resonance can identified (w_n). Using the following equation, the damping ratio (zeta) can be determined:

$$\zeta = \frac{(w_2 - w_1)}{2w_n} \qquad (7.2)$$

All the resonances (natural frequencies) and the F.R.F Imaginary part values for every location have been tabulated in the table below (Table XII).

Table XIII

Resonances and Imaginary values for every location

Pt 1	
Resonance (Hz)	Real Value
4702	0.0115
7677	0.1041
8280	-0.018
9427	0.0648
10827	0.0236
11472	0.0953
12426	0.0197
14360	-0.0061
16867	0.0198

Pt 2	
Resonance (Hz)	Real Value
4707	0.0097
7677	0.1176
8272	0.0168
9430	0.0542
10830	0.0183
11475	0.0990
12426	-0.0105
14360	0.0083
16870	0.0152

Pt 3	
Resonance (Hz)	Real Value
4694	0.0105
7679	0.0355
8272	0.0167
9427	-0.0212
10835	-0.009
11472	0.0928
12434	0.0204
14373	0.0100
16865	0.0032

Pt 4	
Resonance (Hz)	Real Value
4683	0.0074
9398	0.0756
11478	0.0136
12431	0.0060
14341	-0.0019
16867	0.0022

Pt 5	
Resonance (Hz)	Real Value
4683	0.0063
7637	-0.0058
9406	0.0337
11467	-0.0076
12426	0.0064
14341	-0.0031
16748	0.0122

Pt 6	
Resonance (Hz)	Real Value
4680	0.0127
7631	-0.0079
9414	-0.0050
11472	0.0000
12588	-0.0424
14248	-0.0259
16756	-0.018

Pt 7	
Resonance (Hz)	Real Value
4683	0.0173
9411	0.1041
11483	-0.0808
12580	-0.3319
14238	-0.2105
16753	0.0427

Pt 8	
Resonance (Hz)	Real Value
4688	-0.0020
7634	-0.0662
9411	-0.0879
11478	-0.1363
12585	0.6843
14248	0.0138
16756	-0.0236

Pt 9	
Resonance (Hz)	Real Value
4686	-0.0010
7634	-0.0486
9414	-0.0444
11475	-0.0604
12585	0.3202
14246	-0.1055
16753	0.0174

As noticed, the resonances have different frequency values for every tested blade locations. The reason for this is that the setup had to be moved for every location to get focus in the mirrors of the laser vibrometer. Changing the setup introduced a small shift in the natural frequencies of the blade. Some resonances were not identified for certain locations. Either this could be due to a nodal line at that location for that particular mode shape or the displacement was so small that it could be found to be negligible.

The mode shapes were displayed using the "patch" command in MATLAB®. Each corner of the experimental mode shape represents one measure point as shown in Figure 35. The imaginary values were not modified to unity since any further analyses were performed. The experimental mode shapes are presented in the figures below with the associated analytical mode shapes (Figure 35 to Figure 47).
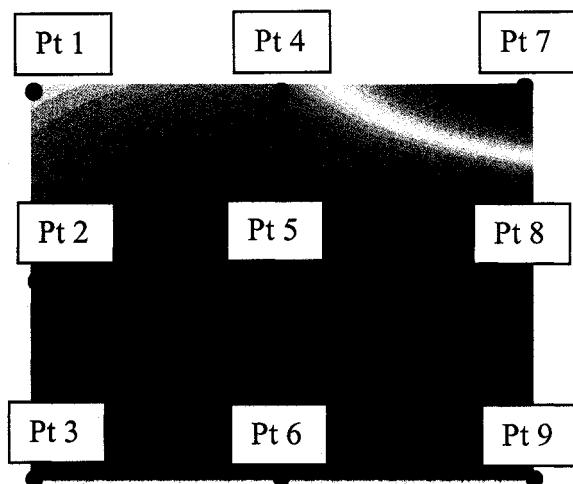
Figure 35 Exp. Mode 1 @ 4689.6 Hz
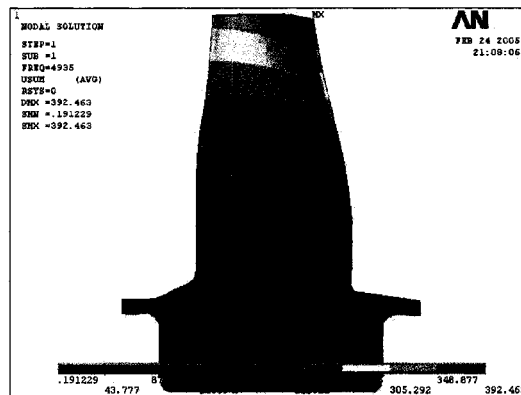
Figure 36   Mode 1 @ 4935 Hz
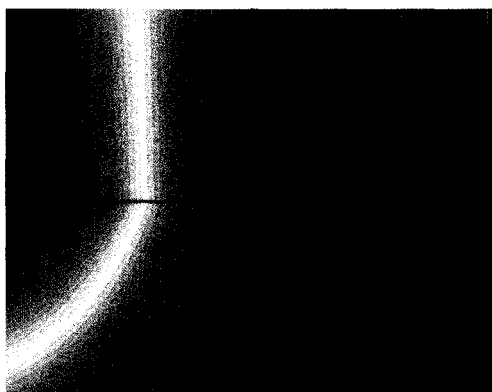
Figure 37   Exp. Mode 2 @ 7652.7 Hz
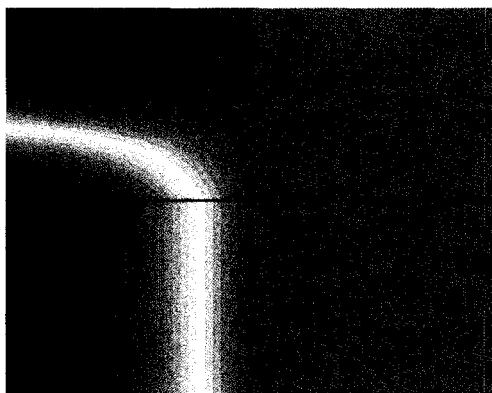
Figure 38   Exp. Mode @ 8272 Hz
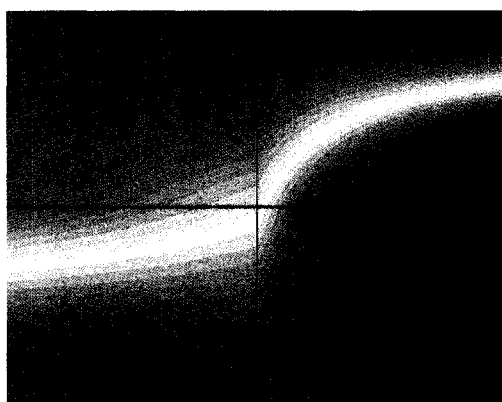
Figure 39   Exp. Mode 4 @ 9415.3 Hz

Figure 40   Exp. Mode 5 @ 10830.7 Hz
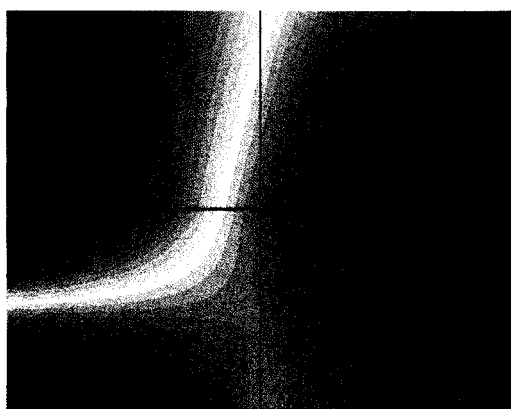
Figure 41   Exp. Mode 6 @ 11474.7 Hz
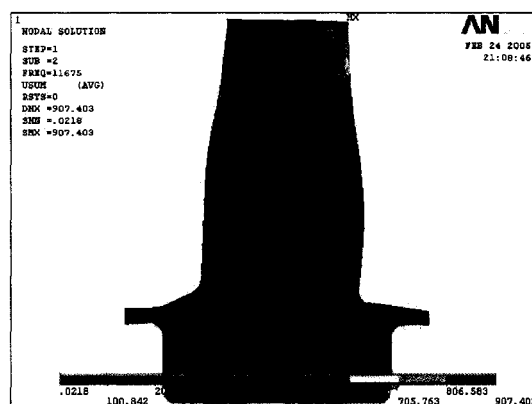
Figure 42   Mode 2 @ 11675 Hz

Figure 43   Exp. Mode 7 @ 12497.9 Hz

Figure 44   Exp. Mode 8 @ 14306.1 Hz
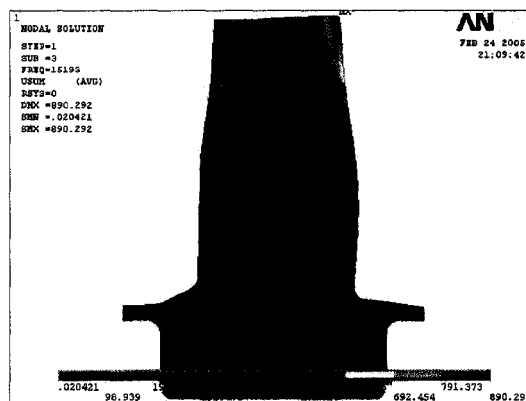
Figure 45   Mode 3 @ 15193 Hz

Figure 46   Exp. Mode 9 @ 16803.9 Hz
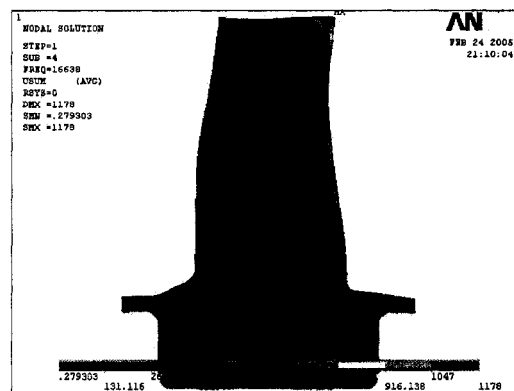
Figure 47   Mode 4 @ 16638 Hz

Nine (9) experimental mode shapes were determined during the testing. The four (4) analytical mode shapes were associated with the corresponding experimental mode shapes. The other five (5) mode shapes not associated with any experimental mode shapes were, either not present for all the locations or are due to the fixing system. The resonances frequency values were averaged for all the location and compared to the analytical resonance frequency values (Table XIII). In addition, the modal damping was extracted from the test data in the damping ratio (zeta) form. It was converted to the decrement logarithmic form using the inverse of equation 7.1.

Table XIV

Experimental and Analytical natural frequencies comparison

Experimental	Analytical	Error	Zeta	Dec. Log.
4689.6	4935	-4.97%	0.088%	0.0055
7652.7	N/A	N/A	N/A	N/A
8272	N/A	N/A	N/A	N/A
9415.3	N/A	N/A	N/A	N/A
10830.7	N/A	N/A	N/A	N/A
11474.7	11675	-1.72%	0.078%	0.0049
12497.9	N/A	N/A	N/A	N/A
14306.1	15193	-5.84%	0.056%	0.0035
16803.9	16638	1.00%	0.015%	0.0009

The analytical natural frequencies were determined using a friction coefficient of 0.1. Although the frequency error was less than 6 %, the modal damping values seem much below the expected range, the data cannot be completely trusted due to the lack of an excited frequency range.

Further study was made to determine the excitable frequency range of the JBL Professional Series Model No. 2425 High Frequency Speaker coupled to a Horn Model No. 2306. Using a control voltage of 0.1 Volt as a power source, the excitable frequency range of the speaker used during the experimental testing was measured using the data acquisition and the microphone. The results are plot in the power form (dB) versus frequency to determine the excitable frequency range (Figure 48).

Test JBL Model No. 2425 Speaker
Coltage Control = 0.1 V

160.00
140.00
120.00
100.00
80.00
60.00
40.00
20.00
0.00
-20.00
-40.00
-60.00
-80.00
-100.00
-120.00
-140.00
-160.00

Power (dB)

2   3   6   11   19   35   63   114   206   372   673   1217   2199   3975   7184   12986
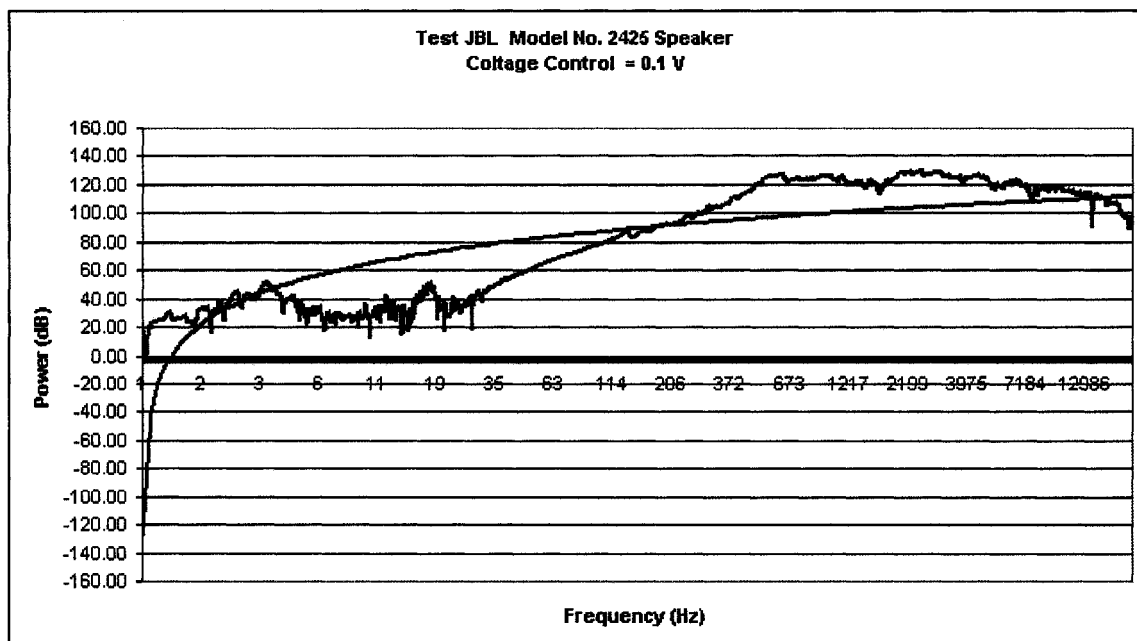
Frequency (Hz)

Figure 48   Excitable range on the JBL High Frequency Speaker

As demonstrated, the JBL Professional Series Model No. 2425 High Frequency Speaker coupled to a Horn Model No. 2306 has only an excitable frequency range of 500 Hz to 12 kHz. Based on the results, a negative slope in power is noticed for frequencies above 12 kHz. Furthermore, the specifications of the Professional Series Model No. 2425 High Frequency Speaker state the excitable frequencies ranges from 500 to 15 kHz (APPENDIX 5). Although there is a drop in power after 12 kHz, JBL state that the speaker is still usable for another 3 kHz. During the experimental testing, the excitable frequencies ranged from 500 Hz to 8 kHz. Therefore, not only the speaker did not have a frequency range sufficient to meet the objective of the testing but also other factors such as the frequency generator, the mixer or the amplifier could have decreased the excitable frequency range from 15 kHz to 12 kHz.

7.4 Analytical Vibratory Stress Prediction Results

Using the FLARES tool, the modal amplification factor was found for every resonance of the PWC Engine 1 HPT Blade, PWC Engine 2 HPT Blade and the PWC Engine 3 CT Blade. To determine the vibratory stress, the modal vibratory stress matrix for a particular mode was multiplied by the associated modal amplification factor. The modal vibratory stress matrix is determined by ANSYS® by using the maximum S1 or S3 strain at each node and then plotting the scaled results. The run file needed to perform a FLARES analysis in presented in the APPENDIX 6.

7.4.1 Results verification

To determine whether the FLARES results are correct, few steps must be undertaken to verify that the mode shapes and the unsteady pressure harmonics are correct.

The mode shape is generated by FLARES by reading the result file obtained from ANSYS® and compared (Figure 49 and 50). Four (4) corner nodes (Leading and trailing edges at the tip and root of the airfoil) must be specified so that the mapping between the modal analysis meshing and the CFD code meshing can be performed on the airfoil only.
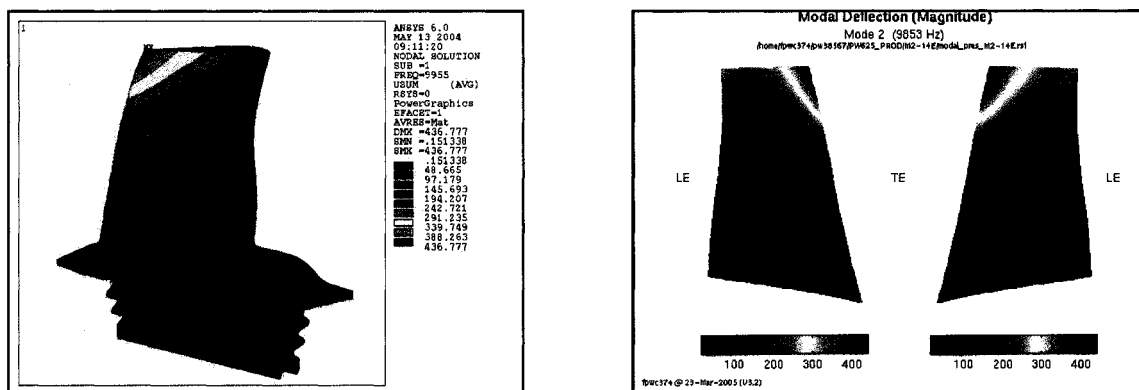
Figure 49   Mode shape comparison between ANSYS and FLARES

When the mode shape generated by FLARES is very close to the one determined by ANSYS®, it certifies that the corner nodes were chosen properly to match the CFD mesh and that the amplification factor obtained with FLARES will be correct.

It is well known that modal force is inversely proportional to the harmonic of unsteady pressure signal. Therefore, the higher the harmonic, the lower the modal force is acting on the airfoil. This has to be verified in order to certify that the aerodynamic solution is valid (Figure 50).
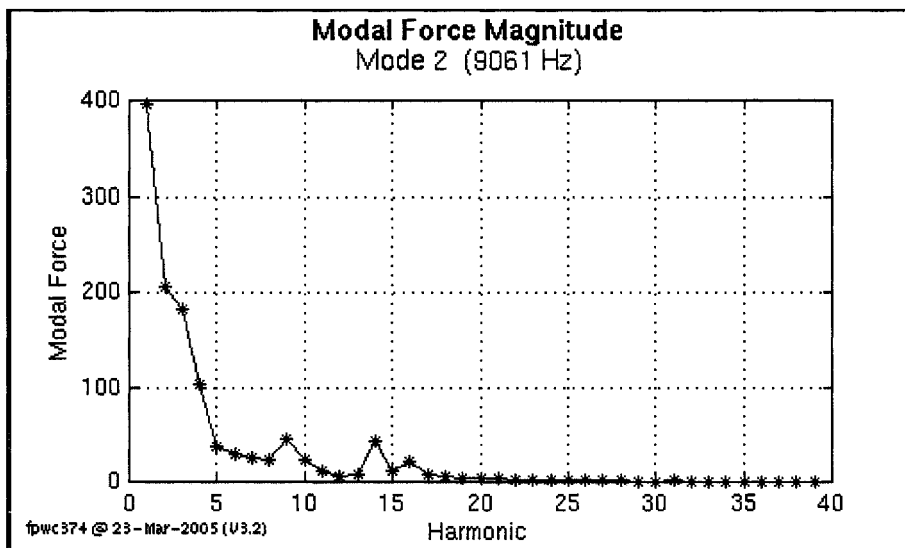
Figure 50   Modal force versus the harmonic of the unsteady pressure signal generated by FLARES

As shown in the figure above, the first harmonic of the excitation on the airfoil has a modal force higher than all the other harmonics. For the harmonics 9, 14 and 16, the error in the analytical results for these very harmonic numbers show a higher modal force than lower harmonic numbers but in reality, these harmonics would have a very small modal force value.

7.4.2 Modal amplification factor results

Based on the data reduction results presented in section 6.1, a modal amplification factor has been determined analytically for each resonance of every engine model HPT or CT blade studied.

Table XV

PWC Engine 1 HPT Blade Analytical Vibratory Stress Comparison

E6211B6 Airfoil		FLARES Amplification Factor	Sensitivity	Predicted Vibratory Stress	WF Stress Error (%)	OA Stress Error (%)	EO Stress Error (%)
Mode	SG						
M2-1H	3E	5.9767E-07	2.0128%	0.180109	-29.04%	53.38%	-0.11%
M4-2H		5.6706E-07	4.6692%	2.163107	81.60%	81.89%	81.71%
M2-1H	1D	5.9614E-07	2.0128%	0.839782	-27.14%	51.00%	-1.18%
M4-2H		5.6706E-07	4.6692%	0.446083	58.13%	72.91%	85.37%
M2-1H	12G	5.9645E-07	2.0128%	1.28863	16.40%	70.42%	29.24%
M4-2H		5.6706E-07	4.6692%	0.926066	82.45%	84.11%	93.11%
M2-1H	5F	6.4089E-07	2.0128%	1.048112	16.15%	68.39%	23.26%
M4-2H		5.6706E-07	4.6692%	1.368599	87.51%	87.88%	87.71%
M2-1H	7M	5.9507E-07	2.0128%	1.303144	-17.89%	76.94%	0.68%
M4-2H		5.6706E-07	4.6692%	1.233242	49.64%	73.53%	91.06%

Fixing		FLARES Amplification Factor	Sensitivity	Predicted Vibratory Stress (ksi)	WF Stress Error (%)	OA Stress Error (%)	EO Stress Error (%)
Mode	SG						
M2-1H	8A	6.4270E-07	2.0128%	1.115663	-17.94%	47.29%	0.50%
M4-2H		5.6706E-07	4.6692%	0.471448	28.37%	71.08%	65.04%
M2-1H	9C	6.1410E-07	2.0128%	0.819025	-6.48%	61.39%	7.68%
M4-2H		5.6706E-07	4.6692%	0.472401	77.13%	81.31%	77.28%

7.4.3 Analytical vibratory stress results interpretation

For the interpretation of the results, the first parameter to analyze is the sensitivity value obtained for each resonance. The maximum sensitivity value found was 4.67% for the whole study. This parameter dictates how much 1% of changes on any of the variables

will have an effect on the modal amplification factor calculation. By rule of thumb, if the sensitivity value is below 5%, the analysis is judged acceptable.

For the PWC Engine 1 HPT Blade, the resonance between the second mode (M2 - Trailing Edge Tip Bending) and the upstream vane passing first harmonic excitation correlates between the analytical and experimental results within 0.11% to 7.68%. Since no resonance was recorded during experimental testing, the vibratory stresses were compared at the maximum engine speed permitted and therefore off-resonance. For the same reason, no total damping value could be extracted and therefore, the total damping value was derived to achieve the minimum error possible. The total damping used to determine the vibratory stresses for the M2-1H had a logarithmic decrement value of 6.39%, which is within PWC's field of experience. The resonance between the fourth mode (M4 – Trailing Edge Second Bending) and the upstream vane passing second harmonic excitation correlates between the analytical and experimental results within 65.04% to 93.11%. The total damping value used (1.64% logarithmic decrement) was obtained for the experimental data. Compared to the other engines, the error margin is above expected for a second harmonic excitation resonance. After investigation, it was found that the steady and unsteady aerodynamic files were generated with an older code and method for this particular case. Therefore, when these aerodynamic files will be generated with the newer version of the CFD code and method, a decrease in the error between the analytical vibratory stress prediction and the experimental vibratory stress will be expected.

For the PWC Engine 2 HPT Blade, the resonance between the second mode (M2 - Trailing Edge Tip Bending) and the upstream vane passing first harmonic excitation correlates between the analytical and experimental results within 19.01% to 370.8%. The total damping value used (3.8% logarithmic decrement) was obtained for the experimental data. Since it was possible to retrieve the experimental data from the strain gage test, the analytical values were compared to values obtained from internal report, which used an older methodology to obtain the vibratory stresses. Therefore, the values

were not correlated with great confidence. The resonance between the fourth mode (M4 – Trailing Edge Second Bending) and the upstream vane passing second harmonic excitation correlates between the analytical and experimental results within 0.08% to 43.73%. The total damping value used (1.55% logarithmic decrement) was obtained for the experimental data. Compared to the other engines, the error margin is within the expected range for a second harmonic excitation resonance.

For the PWC Engine 3 CT Blade, the resonance between the second mode (M2 - Trailing Edge Tip Bending) and the upstream vane passing first harmonic excitation correlates between the analytical and experimental results within 0.02% to 14.05%. Since no resonance was recorded during experimental testing, the vibratory stresses were compared at the maximum engine speed permitted and therefore off-resonance. For the same reason, no total damping value could be extracted and therefore, the total damping value was derived to achieve the minimum error possible. The total damping used to determine the vibratory stresses for the M2-1H had a value of 13.01% logarithmic decrement, which is higher than PWC's field of experience. After investigation, it was found the CFD code could not predict the unsteady flow due to non-linear effects at high engine rotational speed. Therefore, actions have been undertaken to modify the CFD code so that it can predict these phenomenon with better accuracy. The resonance between the fourth mode (M4 – Trailing Edge Second Bending) and the upstream vane passing second harmonic excitation correlates between the analytical and experimental results within 0.87% to 52.58%. The total damping value used (0.924% logarithmic decrement) was obtained for the experimental data. Compared to the other engines, the error margin is within the expected range for a second harmonic excitation resonance.

It was determined that the lowest error margin was from the comparison between the analytical vibratory stress and the engine order (EO) vibratory stress measurement, which was expected. The waterfall value (WF) underestimates the measured vibratory stress due to marginal precision errors in the Fast Fourier Transform when converting a

time domain signal into the frequency domain. The overall value (OA) overestimated the measured vibratory stress since not only it includes the vibratory stress from the main excitation but as well as other vibratory stresses obtained from other sources of excitations. Therefore, the engine order vibratory stress value is the most accurate when considering only one particular source of excitation which is what FLARES does when calculating the vibratory stress of the an harmonic of a particular vane passing frequency.

CONCLUSION

The subject of this thesis was to develop a methodology to predict the vibratory stresses of a turbomachinery turbine blade. The aerodynamic excitation phenomenon was not studied in this research. Furthermore, the turbine blades studied in this research had the characteristics of being unshrouded, uncooled and used mainly in small to medium sized turbomachineries.

This thesis consisted of four principal subjects. The first subject composed of an analysis of experimental results to extract damping values of the turbine blades as well as resonances. A total modal damping database was created for the Compressor Turbine (CT) or High Pressure Turbine (HPT) blades of the following engines: PWC Engine 1, PWC Engine 2 and PWC Engine 3. These damping values were used to determine analytical vibratory stresses with FLARES. Furthermore, resonances were identified during the data reduction and therefore, the experimental vibratory stresses were extracted. These values were used to correlate the analytical vibratory stresses predicted by FLARES.

The second subject elaborated on an analytical method with finite element analysis using contact elements to determine natural frequencies and modes shapes of the turbine blades. It was noticed that the new analysis with contact elements surpassed all expectations with respect to the current analysis being performed at Pratt & Whitney Canada. The natural frequencies were compared with experimental data, and were found to be in good agreement. Furthermore, the mode shapes were compared with the current analysis results, and were found to be the same. Also, the predicted stress in the fir-tree area was found to be lower than the current analysis, which suggests that the contact elements will predict stress with more accuracy in that area. It was also observed that the contact region tends to increase in area size with the pre-stress effects, which has a significant effect on the boundary conditions of the model. Finally, a convergence study was performed on five contact element parameters. It was found that the model was

stable and convergent. Penetration tests should be performed to obtain experimental values to correlate with the model. Furthermore, it should be determined whether the friction coefficient should be the same for all modes.

The third subject described an experimental method to test the blades in a controlled environment to extract natural frequencies, damping, mode shapes and derived coefficient of friction in an attempt to determine the friction coefficient for each mode. The experimental testing was not performed with great success. The main deficiency was the excitable frequency range performed by the high-frequency speaker. The JBL Professional Series Model No. 2425 speaker coupled to a Model No. 2306 horn was only able to excite a frequency range from 3500 to 8000 Hz. Our analytical predictions showed that the first four modes of the tested blade were in the frequency range from 3000 to 17000 Hz. Therefore, the results for the 2nd, 3rd and 4th modes are very questionable. Furthermore, the coherence signal showed weaknesses at multiple frequencies due to the lack excited frequency range. However, nine (9) modes were extracted from the experimental data. The four analytical modes correlated fairly well for the natural frequency and associated mode shade with the experimental results. Furthermore, the modal damping was extracted from the experimental data and was found to be much lower than expected. Although, since the experimental data was found to be questionable, due to an inadequate excitable frequency range, the extraction of the modal damping results are very questionable and therefore, the friction coefficients were not obtained.

Finally, the fourth subject described the comparison between the vibratory stress experimental values and the prediction of vibratory stresses using an analytical tool. Using the FLARES tool, the modal amplification factor was found for every resonance of the PWC Engine 1 HPT Blade, PWC Engine 2 HPT Blade and the PWC Engine 3 CT Blade. To determine the vibratory stress, the modal vibratory stress matrix for a particular mode was multiplied by the modal amplification factor. The modal vibratory stress matrix is determined by ANSYS® by using the maximum S1 or S3 strain at each

node and then plotting the scaled results. To ensure that the results were valid, the mode shape extracted with FLARES was compared to the mode shape given by ANSYS®. In addition, the modal force magnitude was reviewed for every harmonic excitation. After investigation, it was found the CFD code could not predict the unsteady flow due to non-linear effects. Therefore, the vibratory stress levels, due to the resonance between the second mode and the upstream vane passing first harmonic excitation, were predicted with an error margin ranging from 0% to 371%. The vibratory stress levels, due to the resonance between the fourth mode and the upstream vane passing second harmonic excitation, were predicted with an error margin ranging from 0% to 94%. Therefore, it can be determined, that the FLARES analytical tool can predict accurate vibratory stress levels due to a resonance for an unshrouded, uncooled turbomachinery turbine blade fairly well [16,17]. More work needs to be done on the CFD part of the solution to predict more accurate unsteady pressure levels at the higher engine rotating speeds.

APPENDIX 1

Damping Extraction MATLAB Program

APPENDIX 1.1   Damping Extraction: MATLAB Main program

```
clear all;
close all;
%
*******************************************************************
%
%      Program used to minimize the least square function from SGT data.
%      A SDOF function is used to fit the SGT data.
%      The parameters to be found are:      the damping
%                                           the resonance speed
%                                           the static deflection
%
%      Program input: sgt_data ".csv" file from pwcvibs, 1st col= rotor speed, 2nd col=
strain
%      General info in comment (%)
%      Nmin           minimum speed of the range of interest
%      Nmax           maximum speed of the range of interest
%      Tol_damping    termination tolerance on the damping factor
%      Tol_reso_speed       termination tolerance on the resonance speed
%      Tol_defl       termination tolerance on the static deflection
%      Max_iter       maximum number of iteration
%      Log_dec_init   initial value of the damping factor (%)
%      Delta_init     initial value of the static deflection
%
%      Program output: Log_dec     logarithmic decrement (%) = 2 x pi x Dratio
%                      Nc          resonance speed (rpm)
%                      Delta       static deflection
%
% ------------------------------------------------------------------------------
% input
% ------------------------------------------------------------------------------
sgt_data = 'EO_8203_5_12_3J_1H.CSV'
Nmin = 25000;
Nmax = 34438;
Tol_damping = 1E-6;          %[] = default
Tol_reso_speed = 1E-6;
Tol_defl = 1E-6;
Max_iter = 1E50;
Log_dec_init = 0.15;
Delta_init = 0.1;

% ------------------------------------------------------------------------------
```

```
% main program
% ------------------------------------------------------------------------------
global N
global strain
%----------------------------------------
% load the data
%----------------------------------------
data = load (sgt_data);
data_sort=sortrows(data,1);

% filter the data in the speed range
i=1;
while (data_sort(i,1))<Nmin
     i=i+1;
end
Imin=i;

i=1;
while (data_sort(i,1))<Nmax
     i=i+1;
end
Imax=i;

data_red=data_sort(Imin:Imax,:);

N=data_red(:,1);
strain=data_red(:,2);
[max_strain,I_strain]=max(strain);
reso_speed=N(I_strain);

%----------------------------------------
% minimize the least square sum
%----------------------------------------

%     Display - Level of display. off displays no output; iter displays output at each
iteration;
%       final displays just the final output.
%     MaxFunEvals - Maximum number of function evaluations allowed.
%     MaxIter - Maximum number of iterations allowed.
%     TolFun - Termination tolerance on the function value.
%     TolX - Termination tolerance on x.

Dratio_init = Log_dec_init/(2*pi)/100;
```

```
options
optimset('Display',[],'MaxFunEvals',[],'MaxIter',Max_iter,'Tolfun',[],'TolX',[Tol_dampin
g,Tol_reso_speed,Tol_defl])
[var,fval] = fminsearch('least_square',[Dratio_init,reso_speed,Delta_init]);

for i=1:length(N)
        fit(i)=var(3)/((1-N(i)^2/var(2)^2)^2 + 4*var(1)^2*N(i)^2/var(2)^2 )^0.5;
end
half_power=max(fit)/2^0.5;


%---------------------------------------
% post-processing
%---------------------------------------

Log_dec= 2*pi*abs(var(1))*100
Nc=var(2)
Delta=var(3)

figure(1)
plot(N,strain)
hold on
plot(N,fit,'r','LineWidth',2)
hold on
plot ([Nmin,Nmax],[half_power,half_power],'g')

title([sgt_data],'interpreter','none')
xlabel('Rotor speed (rpm)')
ylabel('SGT data (microstrain / ksi)')
legend('SGT data','Curve fitting','Half power')
axis([Nmin, Nmax, 0, 1.15*max_strain])

%---------------------------------------
% save the output file
%---------------------------------------

fid = fopen(strcat(sgt_data,'.out'),'a');
fprintf(fid,'Curve fitting for damping estimation from SGT data\n');
fprintf(fid,'-----------------------------------------------\n');
fprintf(fid,'Input data\n');
fprintf(fid,'----------\n');
fprintf(fid,'Lower speed = %.0f rpm \n',Nmin);
fprintf(fid,'Upper speed = %.0f rpm \n',Nmax);
fprintf(fid,'Tolerance on the damping = %4.2e \n',Tol_damping);
fprintf(fid,'Tolerance on the resonance speed = %4.2e \n',Tol_reso_speed);
```

```
fprintf(fid,'Tolerance on the static deflection = %4.2e \n',Tol_defl);
fprintf(fid,'Maximum number of iterations = %4.2e \n',Max_iter);
fprintf(fid,'Initial value of the log. dec. = %4.2e \n',Log_dec_init);
fprintf(fid,'Initial value of the static deflection = %4.2e \n',Delta_init);
fprintf(fid,'-----------\n');
fprintf(fid,'SGT data\n');
fprintf(fid,'-----------\n');
fprintf(fid,'SGT Resonance speed = %.0f rpm \n',reso_speed);
fprintf(fid,'Max amplitude = %.2f \n',max_strain);
fprintf(fid,'-----------\n');
fprintf(fid,'Output data\n');
fprintf(fid,'-----------\n');
fprintf(fid,'Log. decrement = %.3f %% \n',Log_dec);
fprintf(fid,'Resonance speed = %.0f rpm \n',Nc);
fprintf(fid,'Static deflection = %.3f \n',Delta);
fprintf(fid,'----------------------------------------------------\n\n');
```

APPENDIX 1.2   Damping Extraction: MATLAB Least square function

```
function f=least_square(x)

global N
global strain

% x(1) = damping factor zeta
% x(2) = resonance speed
% x(3) = static deflection

for i=1:length(N)
        least(i)=(strain(i) - x(3)/((1-N(i)^2/x(2)^2)^2 + 4*x(1)^2*N(i)^2/x(2)^2 )^0.5)^2;
end
f=sum(least);
```

APPENDIX 2

Engine Resonant Frequencies Results

Table XVI

PWC Engine 2 Resonant Frequencies

E5401B11
Airfoil   RPM

Mode	SG	Run	Frequency	N2
M4-2H	13K	8203/1/1.2	1.0	29940
M4-2H	14A	8203/1/1.2	1.002	29961

E5401B13
Airfoil   RPM

Mode	SG	Run	Frequency	N2
M2-1H	8O	8203/5/2	0.582	34777
M4-2H		8203/5/4	1.018	30421

Fixing   RPM

Mode	SG	Run	Frequency	N2
M2-1H	10H	8203/5/3	0.582	34787
M4-2H		8203/5/3	1.030	30793
M2-1H	12E	8203/5/3	0.582	34786
M4-2H		8203/5/3	1.018	30430

E5401B14
Airfoil   RPM

Mode	SG	Run	Frequency	N2
M2-1H	1A	8203/5/13	0.576	34428
M4-2H		8203D/5/12	0.990	29525
M2-1H	3J	8203/5/12	0.576	34418
M4-2H		8203D/5/12	1.008	30180
M2-1H	8O	8203/5/12	0.576	34420
M4-2H		8203/5/12	1.020	30475

Table XV (continued)

E5401B43

Airfoil RPM

Mode	SG	Run	Frequency	N2
M2-1H	5A	8304/1/2	0.586	35079
M4-2H		8304/1/2	0.980	29302
M2-1H	7J	8304/1/2	0.586	35082
M4-2H		8304/1/2	0.942	28184

Fixing RPM

Mode	SG	Run	Frequency	N2
M2-1H	3E	8304/1/2	0.586	35041
M4-2H		8304/1/2	0.964	28836

Table XVII

PWC Engine 3 Resonant Frequencies

E584B19T - Certification SGT – Non-cutback Blade

Airfoil   RPM

Mode	SG	Run	Frequency	Ng
M2-1H	8F	1955/1/3	1.0	42424
M4-2H		1955/1/3	1.724	36565
M2-1H	9A	1955/1/3	1.003	42471
M4-2H		1955/1/3	1.700	36080
M4-2H	11B	1955/2/8	1.645	34984

E584B23T - Axial gap reduced by 0.143in

Airfoil   RPM

Mode	SG	Run	Frequency	Ng
M4-2H	14B	1955/6/37	1.690	35837
M4-2H	3E	1955/6/37	1.714	36341
M4-2H	7C	1955/5/33	1.735	36781
M4-2H	8F	1955/5/33	1.763	37385

Fixing   RPM

Mode	SG	Run	Frequency	Ng
M4-2H	11H	1955/6/37	1.707	36193
M4-2H	12I	1955/6/37	1.721	36491

E584B27 - Axial gap increased by .250in

Airfoil   RPM

Mode	SG	Run	Frequency	Ng
M4-2H	3E	1982/1/3	1.735	36777
M4-2H	7C	1982/1/3	1.697	35956
M4-2H	8F	1982/1/3	1.725	36537

APPENDIX 3

Engine Modal Damping Results

Table XVIII

PWC Engine 2 Modal Damping

Mode	M2		M4	
Excitation	1H		2H	
Harmonic	1st		2nd	
Damping	Dec. Log.	Zeta (%)	Dec. Log.	Zeta (%)
Data	0.0380	0.605%	0.0160	0.255%
			0.0150	0.239%
Average	0.0380	0.605%	0.0155	0.247%
Q value	82.65		202.43	
Variance	0.00E+00	0.00E+00	5.00E-07	1.27E-08

Table XIX

PWC Engine 3 Modal Damping

Mode	M2		M3		M4	
Excitation	2H		2H		2H	
Harmonic	2nd		2nd		2nd	
Damping	Dec.	Zeta (%)	Dec.	Zeta (%)	Dec.	Zeta (%)
Data	0.0108	0.172%	0.0075	0.119%	0.0088	0.140%
	0.0117	0.186%	0.0089	0.142%	0.0102	0.162%
	0.0142	0.226%	0.0111	0.177%	0.0117	0.186%
	0.0142	0.226%	0.0115	0.183%	0.0123	0.196%
	0.0172	0.274%	0.0120	0.191%	0.0136	0.216%
	0.0193	0.307%	0.0170	0.271%	0.0146	0.232%
			0.0265	0.422%	0.0292	0.465%
Average	0.0146	0.232%	0.0135	0.215%	0.0143	0.228%
Q value	215.52		232.56		219.30	
Variance	1.04E-05	1.59E-07	4.17E-05	1.06E-06	4.67E-05	8.81E-08

APPENDIX 4

Engine Vibratory Stress Results

Table XX

PWC Engine 2 Vibratory Stress

E5401B11

Airfoil

			RPM	ksi	ksi	ksi
Mode	**SG**	**Frequency**	**N2**	**WF stress**	**OA stress**	**EO stress**
M4-2H	13K	1.0	29940	7.8574	9.6255	N/A
M4-2H	14A	1.002	29961	1.4630	2.2273	N/A

E5401B13

Airfoil

			RPM	ksi	ksi	ksi
Mode	**SG**	**Frequency**	**N2**	**WF stress**	**OA stress**	**EO stress**
M2-1H	8O	0.582	34777	2.9740	3.3566	N/A
M4-2H		1.018	30421	2.4970	2.9426	N/A

Fixing

			RPM	ksi	ksi	ksi
Mode	**SG**	**Frequency**	**N2**	**WF stress**	**OA stress**	**EO stress**
M2-1H	10H	0.576	34787	2.4706	2.6543	N/A
M4-2H		0.990	30793	0.3093	1.0807	N/A
M2-1H	12E	0.576	34786	3.0228	3.2197	N/A
M4-2H		1.008	30430	2.5524	2.8699	N/A

E5401B14

Airfoil

			RPM	ksi	ksi	Ksi
Mode	**SG**	**Frequency**	**N2**	**WF stress**	**OA stress**	**EO stress**
M2-1H	1A	0.576	34428	4.1495	4.4425	N/A
M4-2H		1.020	29525	1.3851	2.2161	N/A
M2-1H	3J	0.576	34418	9.9026	10.1742	N/A
M4-2H		1.008	30180	3.0730	3.5904	N/A

Table XIX (continued)

E5401B43

Airfoil

			RPM	ksi	ksi	ksi
Mode	**SG**	**Frequency**	**N2**	**WF stress**	**OA stress**	**EO stress**
M2-1H	5A	0.586	35079	5.5294	5.9275	N/A
M4-2H		0.980	29302	1.1279	1.9367	N/A
M2-1H	7J	0.586	35082	11.0312	12.1177	N/A
M4-2H		0.942	28184	3.5722	4.2304	N/A

Fixing

			RPM	ksi	ksi	ksi
Mode	**SG**	**Frequency**	**N2**	**WF stress**	**OA stress**	**EO stress**
M2-1H	3E	0.586	35041	7.8357	8.1571	N/A
M4-2H		0.964	28836	1.7832	2.2083	N/A

Table XXI

PWC Engine 3 Vibratory Stress

E584B19T - Certification SGT

Airfoil   RPM   ksi   ksi   ksi

Mode	SG	Frequency	Ng	WF stress	OA stress	EO stress
M2-1H	8F	1.0	42424	6.0311	7.9321	6.5055
M4-2H		1.724	36565	17.0119	18.2910	17.8431
M2-1H	9A	1.003	42471	1.3524	2.6488	1.6953
M4-2H		1.700	36080	0.4373	2.1446	2.4339
M4-2H	11B	1.645	34984	1.5538	1.8449	1.9208

E584B23T - Axial gap reduced by 0.143in

Airfoil   RPM   ksi   ksi   ksi

Mode	SG	Frequency	Ng	WF stress	OA stress	EO stress
M4-2H	14B	1.690	35837	9.9339	11.4686	11.4538
M4-2H	3E	1.714	36341	21.3722	22.8474	23.0191
M4-2H	7C	1.735	36781	7.3111	8.4139	7.9293
M4-2H	8F	1.763	37385	9.2260	11.0369	9.7144

Fixing   RPM   ksi   ksi   ksi

Mode	SG	Frequency	Ng	WF stress	OA stress	EO stress
M4-2H	11H	1.707	36193	1.3213	2.0222	2.3283
M4-2H	12I	1.721	36491	1.1990	1.8251	1.2619

E584B27 - Axial gap increased by .250in

Airfoil   RPM   ksi   ksi   Ksi

Mode	SG	Frequency	Ng	WF stress	OA stress	EO stress
M4-2H	3E	1.735	36777	17.6550	18.1889	18.0827
M4-2H	7C	1.697	35956	3.9194	4.6422	3.4017
M4-2H	8F	1.725	36537	15.0558	19.2695	16.6901

APPENDIX 5

JBL Speaker Specifications

Specifications

Horn Throat Diameter	25 mm	1 in
Nominal Impedance[1]	16Ω	
Power Capacity[1]	30 watts continuous program	
Sensitivity[2]	117 dB	
Frequency Range	500 Hz to 15 kHz	
Recommend Crossover[3]	800 Hz or Higher	
Diaphragm	0.05 mm (0.002 in) aluminum alloy	
Voice Coil Diameter	44 mm	1 3/4 in
Voice Coil Material	Edgewound aluminum ribbon	
Flux Density	1.6 T (16,000 gauss)	
Bl Factor	8.7 T*m	
Dimensions	114 mm (4 ½ in) diameter	
	98 mm (3 7/8 in) depth	
Net Weight	3.7 kg	8 1/8 lb
Shipping Weight	4.0 kg	8 3/4 lb

[1] Continuous program power is defined as 3 dB greater than continuous sine wave power (RMS). It is conservative expression of the transducers ability to handle normal speech and music program material.

[2] As specified by recognized organizations, sensitivity is measured with the driver coupled to a terminated tube. The JBL rating represents the SPL in a 25 mm (1-in) diameter tube with a 1mW input signal (0.126 volts into 16 ohms) warbled from 500 Hz to 2500 Hz.

[3] A 2410 can be used to 500 Hz; however, power capacity will be reduced to 10 watts continuous program in the region between 500 Hz and 800 Hz.

APPENDIX 6

FLARES Input File

```
$-------------------------------------------------------------------------
$
$ FLARES INPUT FILE FORMAT
$ INPUT IS CONTROLED BY KEYWORDS: ALL CAPITAL LETTERS ENDING IN =
$                    FOLLOWED BY AT LEAST ONE BLANK THEN INPUT
$                    LINE LIMIT: 630 CHARACTERS
$                    PATH LIMIT: 500 CHARACTERS
$ KEYWORDS MAY BE IN ANY ORDER
$ DATA CHECKING IN res.auxin.echo
$ COMMENT CARDS BEGIN WITH $ or > , BLANK LINES ARE ALLOWED
$
$-------------------------------------------------------------------------
$
$*************************************************************************
$      REQUIRED INPUT
$-------------------------------------------------------------------------
$
$----------------------------------
$ Input to be used with ANSYS standard run file
$ FEM Cartesian CS - Z = Engine axis from LE to TE - X = Stacking axis
IBTYPE= 5
ICORD= 2
ICOMPL= 0
NSUBC= 0
$
$----------------------------------
$ Path to ANSYS .rst File
ANSFILE= /home/fpwc374/pw38567/PW625_FER/M2-1H/modal_pres_M2-1H.rst
$
$----------------------------------
$ Airfoil RLE, RTE, TLE & TTE FEM Grid Point Numbers
IRLE= 94945
IRTE= 132587
ITLE= 258
ITTE= 93026
$
```

```
$-----------------------------------
$ Actual Number of Blades for Vibratory Stress Prediction or Flutter
NB= 55
$
$-----------------------------------
$ Aerodynamic and Mechanical Damping (Logarithmic decrement)
DAERO= 0.005911
DMECH= 0.019089
$
$-----------------------------------
$ Path to the unsteady CFD input file (from Aero)
CFDIN= /home/fpwc374/pw38567/PW625_FER/M2-1H/pw625_prod_flares_RLS_notip.dat
$
$-----------------------------------
$ Mechanical Speed of Unsteady CFD Analysis
CFD_SPD= 36160.0
$
$-----------------------------------
$ Path to Pressure vs. RPM Table for Scaling CFD Loads (from Performance)
PRESSURE= /home/fpwc374/pw38567/PW625_FER/M2-1H/PvsN.dat
$
$-----------------------------------
$ Engine Order(s) to be analyzed
EO= 14.0
$
$-----------------------------------
$ Harmonics of CFD Time History that Model the Engine Order(s)
NUHARM= 1
$
$-----------------------------------
$ Mode Number to Analyze
$ NMODE = 0 => Analyze All Modes in [RPM_LOWER , RPM_UPPER]
NMODE= 2
>RPM_LOWER= 12000.
>RPM_UPPER= 20900.
$
```

```
$------------------------------------------------------------------------
$       END OF REQUIRED INPUT
$***********************************************************************
$
$
$***********************************************************************
$       OPTIONAL INPUT
$------------------------------------------------------------------------
$
$------------------------------------
$ Reverse Rotation Direction of CFD airfoil input to Align with FEM airfoil
$  0 : Do Nothing (Default)
$  1 : Reverse CFD Airfoil Rotation Direction
ICNTROT= 0
$
$------------------------------------
$ Path to Frequency vs. RPM Table for Calculating Resonance Speed
$ Available only at PWEH
SPEED_FREQ= /home/fpwc374/pw38567/PW625_FER/M2-1H/pw625_fvsRPM.dat
$
$------------------------------------
$ Path to the File Containing Grid or Element List for Stress Calculation
>SGIN=
$
$------------------------------------------------------------------------
$       END OF OPTIONAL INPUT
$***********************************************************************
$
$
$***********************************************************************
$       REQUIRED ONLY FOR LUNAR AERO DAMPING
$------------------------------------------------------------------------
$
$------------------------------------
$ Calculate Aerodynamics Damping Using LUNAR
$  0 : No LUNAR Calculation (Default)
```

$ 1 : LUNAR Calculation

$ 9999 : Number of LUNAR iterations (available at PWEH only)

NLUNAR= 0

$

$-----------------------------------

$ Path to Y237 Steady Euler Restart File for LUNAR

>STEADYIN= /home/fpwc374/pw38567/PW625_FER/M2-1H/pw625_prod_lunar_RLS_12_02.binary

$

$--

$ END OF REQUIRED ONLY FOR LUNAR AERO DAMPING

$***

$

$

$ Last Line of res.auxin File

%END OF FILE%

APPENDIX 7

Engine Vibratory Stress Analytical Prediction Results

Table XXII

PWC Engine 2 Analytical Vibratory HPT Blade Stress Comparison

E5401B11 Airfoil		FLARES Amplification Factor	Sensitivity	Predicted Vibratory Stress (ksi)	WF Stress Error (%)	OA Stress Error (%)	EO Stress Error (%)
Mode	SG						
M4-2H	13K	1.6016E-06	2.1795%	10.39839	-32.34%	-8.03%	**-18.95%**
M4-2H	14A	1.6016E-06	2.1795%	1.533596	-4.82%	31.15%	**16.89%**

E5401B13 Airfoil		FLARES Amplification Factor	Sensitivity	Predicted Vibratory Stress (ksi)	WF Stress Error (%)	OA Stress Error (%)	EO Stress Error (%)
Mode	SG						
M2-1H	8O	9.2446E-06	1.5449%	8.749737	-194.2%	-161%	**-176.4%**
M4-2H		1.6016E-06	2.1795%	3.608725	-44.52%	-22.6%	**-32.68%**

Fixing		FLARES Amplification Factor	Sensitivity	Predicted Vibratory Stress (ksi)	WF Stress Error (%)	OA Stress Error (%)	EO Stress Error (%)
Mode	SG						
M2-1H	10H	9.2446E-06	1.5449%	7.548216	-205.5%	-184%	**-194.6%**
M4-2H		1.6016E-06	2.1795%	0.828332	-167.8%	23.35%	**-19.20%**
M2-1H	12E	9.2446E-06	1.5449%	14.69799	-386.2%	-357%	**-370.8%**
M4-2H		1.6016E-06	2.1795%	1.987586	22.13%	30.74%	**26.72%**

E5401B14 Airfoil		FLARES Amplification Factor	Sensitivity	Predicted Vibratory Stress (ksi)	WF Stress Error (%)	OA Stress Error (%)	EO Stress Error (%)
Mode	SG						
M2-1H	1A	9.2446E-06	1.5449%	11.48826	-176.9%	-159%	**-167.4%**
M4-2H		1.6016E-06	2.1795%	1.533596	-10.72%	30.80%	**14.83%**
M2-1H	3J	9.2446E-06	1.5449%	13.7763	-39.12%	-35.4%	**-37.22%**
M4-2H		1.6016E-06	2.1795%	2.21181	28.02%	38.40%	**33.62%**
M2-1H	8O	9.2446E-06	1.5449%	8.745392	-86.26%	-75.9%	**-80.93%**
M4-2H		1.6016E-06	2.1795%	3.608725	-68.99%	-25.1%	**-43.73%**

Table XXI (continued)

E5401B43 Airfoil		FLARES Amplification Factor	Sensitivity	Predicted Vibratory Stress (ksi)	WF Stress Error (%)	OA Stress Error (%)	EO Stress Error (%)
Mode	SG						
M2-1H	5A	9.2446E-06	1.5449%	11.4633	-107.3%	-93.4%	**-100.1%**
M4-2H		1.6016E-06	2.1795%	1.533596	-35.96%	20.82%	**-0.08%**
M2-1H	7J	9.2446E-06	1.5449%	13.77445	-24.87%	-13.7%	**-19.01%**
M4-2H		1.6016E-06	2.1795%	2.21181	38.08%	47.72%	**43.32%**
Fixing		FLARES Amplification Factor	Sensitivity	Predicted Vibratory Stress (ksi)	WF Stress Error (%)	OA Stress Error (%)	EO Stress Error (%)
Mode	SG						
M2-1H	3E	9.2446E-06	1.5449%	14.69891	-87.59%	-80.2%	**-83.81%**
M4-2H		1.6016E-06	2.1795%	1.985984	-11.37%	10.07%	**0.52%**

Table XXIII

PWC Engine 3 Analytical Vibratory CT Blade Stress Comparison

E584B19T: Certification SGT - Non-cutback Blade

Airfoil		FLARES Amplification Factor	Sensitivity	Predicted Vibratory Stress (ksi)	WF Stress Error (%)	OA Stress Error (%)	EO Stress Error (%)
Mode	SG						
M2-1H	8F	1.3570E-06	1.6253%	6.504372	-7.85%	18.00%	0.02%
M4-2H		2.1281E-06	2.3630%	21.54276	-26.63%	-17.78%	-20.73%
M2-1H	9A	1.3714E-06	1.6253%	1.933537	-42.97%	27.00%	-14.05%
M4-2H		2.1281E-06	2.3630%	3.487956	-697.6%	-62.64%	-43.31%
M4-2H	11B	2.1281E-06	2.3630%	2.681406	-72.57%	-45.35%	-39.60%

E584B23T: Axial gap reduced by 0.143in

Airfoil		FLARES Amplification Factor	Sensitivity	Predicted Vibratory Stress (ksi)	WF Stress Error (%)	OA Stress Error (%)	EO Stress Error (%)
Mode	SG						
M4-2H	14B	2.1284E-06	1.4268%	10.52834	-5.98%	8.20%	8.08%
M4-2H	3E	2.1284E-06	1.4268%	21.93955	-2.65%	3.97%	4.69%
M4-2H	7C	2.1284E-06	1.4268%	9.462654	-29.43%	-12.4%	-19.34%
M4-2H	8F	2.1284E-06	1.4268%	13.26866	-43.82%	-20.2%	-36.59%

Fixing		FLARES Amplification Factor	Sensitivity	Predicted Vibratory Stress (ksi)	WF Stress Error (%)	OA Stress Error (%)	EO Stress Error (%)
Mode	SG						
M4-2H	11H	2.1284E-06	1.4268%	2.59154	-96.14%	-28.2%	-11.31%
M4-2H	12I	2.1284E-06	1.4268%	1.383928	-15.43%	24.17%	-9.67%

E584B27: Axial gap increased by .250in

Airfoil		FLARES Amplification Factor	Sensitivity	Predicted Vibratory Stress (ksi)	WF Stress Error (%)	OA Stress Error (%)	EO Stress Error (%)
Mode	SG						
M4-2H	3E	8.0074E-07	1.6845%	8.509464	51.80%	53.22%	52.52%
M4-2H	7C	8.0074E-07	1.6845%	4.156641	-6.05%	10.46%	-0.87%
M4-2H	8F	8.0074E-07	1.6845%	8.105891	46.16%	57.93%	47.82%

BIBLIOGRAPHY

[1]   NASA/GUIde. NASA/GUIde Consortium Industry Survey.

[2]   Hilbert, G. R., Ni, R.-H., & Takahashi, R. K. (1997). *Forced response prediction of gas turbine rotor blades.* Paper presented at the Proceedings of the 1997 ASME International Mechanical Engineering Congress and Exposition, Nov 16-21 1997, Dallas, TX, USA.

[3]   Ishihara, K. Vibration of turbomachine-blade due to viscous wakes. Strength Research Laboratory, Technical Institute, Kawasaki Heavy Industries Ltd., Akashi, Japan, 13.

[4]   Hilditch, M. A., Smith, G. C., & Singh, U. K. (1998). Unsteady flow in a single stage turbine. *The American Society of Mechanical Engineers, 98-GT-531*, 10.

[5]   Krysinki, J. E., Blaszczak, J. R., Smolny, A., & Gallus, H. E. 3D Unsteady Flow Experimental Investigations in a Two-Stage Low-Pressure Model Turbine. *ASME*, 515-523.

[6]   Jöcker, M., K., F., Fransson, T. H., & Rehder, H.-J. Parametric Studies of the Aerodynamic Excitation in High Pressure Turbines. 537-558.

[7]   Clark, J. P. A. A. S. V., M. A. ; Gacek R. E. ; Magge S. S. ; Price F. R. (2002). Using CFD to Reduce Resonant Stresses on a Single-Stage High-Pressure Turbine Blade. *ASME*, 7.

[8]   Meguid, S. A., Kanth, P. S., & Czekanski, A. (2000). Finite element analysis of fir-tree region in turbine discs. *Finite Elements in Analysis and Design, 35*(4), 305-317.

[9]   Cescotto, S. & Charlier, R. (1993). Frictional Contact Finite Elements Based On Mixed Variational Principles. *International Journal For Numerical Methods in Engineering*, 20.

[10]   Berger, E. J. & Phadke, R. (2005). Microslip Damping Analysis with a User-Programmed Functio in Ansys. *10th National Turbine Engine HCF Conference*, New Orleans, NV, March 2005.

[11]   Li, J., Pierre, C. & Ceccio, S.L. (2005). Validation of a New Technique for Mistuning Identification and Model Updating Based on Experimental Results for an Advanced Bladed Disk Prototype. In *Evaluation, Control and Prevention of High Cycle Fatigue in Gas Turbine Engines for Land, Sea and Air Vehicule* (Paper 36). Meeting Proceedings RTO-MP-AVT-121, Neilly-sur-Seine, France: RTO, 16.

[12]   Jay, R. L., MacBain, J. C., & Burns, D. W. (1983). Structural Response due to Blade Vane Interaction. *The American Society of Mechanical Engineers* (83-GT-133), 7.

[13]   Moffat, S. H., Li. (2003). Blade Forced Response Prediction for Industrial Gas Turbines. *ASME, GT2003-28640*, 8.

[14]   Busby, J. A., Davis, R. L., Dorney, D. J., Dunn, M. G., Haldeman, C. W., Abhari, R. S., et al. (1998). Influence of Vane-Blade Spacing on Transonic Turbine Stage Aerodynamics Part II: Time-Resolved Data and Analysis. *The American Society of Mechanical Engineers* (98-GT-482), 11.

[15]   Thomas M., (1976). Optimalisation de la matrice modale d'une structure quelconque, *Sherbrooke University, Departement of mechanical engineering*, Master Thesis IV 177.

[16]   Guerra M., Thomas M. and St-Georges L. (2004). Turbomachinery Turbine Blade Modal Analysis using Contact Elements, SAE 2004, *Transactions Journal of Aerospace*, Vol. 1, paper 2004-01-3141, 1729-1734.

[17]   Guerra M., Thomas M. and David E. (2005). Turbomachinery Turbine Blade Vibratory Stress Prediction using Contact Elements Modeling, *Evaluation, Control and Prevention of High Cycle Fatigue in Gas Turbine Engines for Land, Sea and Air Vehicles*, Meeting Proceedings RTO-MP-AVT-121, Paper 26, Neilly-sur-Seine, France: RTO, 26-1 – 26-12.

[18]   ANSYS (2001). Basic Structural Nonlinearities Training Manual, Release 6.0, 1st Edition, SAS IP.